ICE MARGIN OSCILLATIONS DURING DEGLACIATION OF THE NORTHERN IRISH SEA BASIN

ICE MARGIN OSCILLATIONS DURING DEGLACIATION OF THE NORTHERN IRISH SEA BASIN

R.C. Chiverrell[1*], R.K. Smedley[1,], D. Small[2], C.K. Ballantyne[3], M.J. Burke[1], S.L. Callard[2], C.D. Clark[4], G.A.T. Duller[5], D.J.A. Evans[2], D. Fabel[6], K. van Landeghem[7], S. Livingstone[4], Ó Cofaigh, C.[2], G.S.P. Thomas[1]. D.H. Roberts[2], M Saher[7], J.D. Scourse[8], P. Wilson[9]

[1]School of Environmental Sciences, University of Liverpool, Liverpool, UK

[2]Department of Geography, Durham University, Durham, UK

[3]School of Geography and Sustainable Development, University of St Andrews, St Andrews, UK

[4]Department of Geography, University of Sheffield, Sheffield, UK

[5]Department of Geography and Earth Sciences, Aberystwyth University, Ceredigion, UK

[6]Scottish Universities Environmental Research Centre, East Kilbride, UK

[7]School of Ocean Sciences, Bangor University, Menai Bridge, Anglesey, UK

[8]College of Life and Environmental Science, University of Exeter, Cornwall, UK

[9]School of Geography and Environmental Sciences, University of Ulster, Coleraine, UK

(*E-mail: RCHIV@LIV.AC.UK)

ABSTRACT

We present a new chronology to constrain ice-margin retreat in the northern Irish Sea Basin. Estimates on the timing of ice thinning derived from surface exposure ages for boulders from the summits of the Isle of Man and southwest Cumbria suggest that ice thinning was commensurate with the rapid retreat that followed the short-lived advance of the Irish Sea Ice Stream (ISIS) to maximum limits in the Celtic Sea. This ice retreat in the northern ISB was fastest at 20 ka in response to a wider calving margin, but slowed as ice stabilised and oscillated against the Isle of Man. We provide the first age constraints for the Scottish Readvance (19.2-18.2 ka) and demonstrate that it was a potentially regional event across the Isle of Man and Cumbrian lowlands not linked with Heinrich Event 1. After the Scottish Readvance, the ice front retreated northwards towards the Southern Uplands of Scotland at the same time as climate north of ~45 °N warmed in response to summer insolation. This sequence demonstrates the importance of internal dynamics in controlling ice retreat rates in the Irish Sea, but also that deglaciation of the northern ISB was a response to climate warming.

KEYWORDS: British-Irish Ice Sheet; Irish Sea Ice Stream; Heinrich Event 1; luminescence dating; cosmogenic nuclide dating.

PAPER: 8700 WORDS

1. INTRODUCTION

During the Late Devensian (Marine Isotope Stage 2), ice flowed into the northern Irish Sea Basin (NISB) from Ireland, SW Scotland and the English Lake District (Fig. 1). From the subglacial bedform record in the NISB and surrounding areas, Livingstone et al. (2012) identified flowsets that represent three phases of ice movement. The earliest (Phase I) flow of ice from southwest Scotland and the Lake District extended both southwards across the NISB and eastwards through the Tyne and Stainmore Gaps in northern England. The extensive subglacial bedforms of Phase II indicate northeastwards migration of an ice divide across the Carlisle lowlands, and the development of convergent ice flows west and southwest into the NISB during draw-down of the Irish Sea Ice Stream (ISIS) (Livingstone et al., 2012). This pattern conforms with evidence on the Isle of Man (Roberts et al., 2007) and from the central Irish Sea (Van Landeghem et al., 2009). The bedforms attributed to Phase III indicate that unconfined southerly flow of ice from southwest Scotland reached the Carlisle lowlands and deposited ice-marginal landforms (Livingstone et al., 2010c) that have been attributed to the Scottish Readvance originally proposed by Trotter et al. (1937).

The NISB is bathymetrically asymmetric, reaching depths of - 45 m in the west but shallowing to - 40 m in the east (Fig. 1). In the Solway Firth, a east-west aligned basin descends gradually over ~100 km to a depth of -65 m, then steeply to -145 m in western part of the main basin. Global isostatic adjustment modelling (GIA) by Bradley et al. (2011) suggests that between 24 ka and 16 ka relative sea levels were ~30 m below present, implying that the ISIS had a marine-terminating margin in the western part of the NISB, but may in part have had a terrestrial margin in the east. Smedley et al. (2017a) have shown that retreat of the ISIS margin from the southern Irish Sea Basin was complete by 20.3 ± 0.6 ka; it follows that deglaciation of the NISB coincided with summer insolation-related warming at ~45°N (Bintanja et al., 2005) and overlapped the timing of peaks in ice-rafted debris flux to the southern Celtic Sea associated with Heinrich Event 1 (H1) (Haapaniemi et al., 2010).

The NISB was subjected to multiple standstills or minor (0.1 - 1 km) readvances of the ice margin during deglaciation of differing palaeoclimatic significance (e.g. Thomas et al., 2004). This deglacial signature is recorded in extensive seafloor sediments (Pantin et al., 1978) and in adjacent terrestrial sediments and landforms (Livingstone et al., 2008, 2010a; Livingstone et al., 2010c; Livingstone et al., 2012; McCabe, 2008; Merritt and Auton, 2000; Thomas, 1977; Thomas et al., 2004). The eastern and western Irish Sea mud belts (Jackson et al., 1995; Pantin et al., 1978) are basins filled with substantial thicknesses (>10 m) of Holocene sediment and bury the glacial stratigraphy. The Holocene sediment fill in the Solway Firth is thinner, and there is a greater potential for the visibility of glacigenic landforms on the sea floor (Jackson et al., 1995; Pantin et al., 1978). The morpho-stratigraphical evidence for movements of the ice margins includes multiple

advance-retreat cycles on the Isle of Man (Thomas, 1977, 1984; Thomas et al., 2004; Thomas et al., 2006), and the Gosforth and Scottish Readvances in northwest England (Huddart, 1971, 1977; Huddart and Glasser, 2002; Livingstone et al., 2008; Livingstone et al., 2010b; Livingstone et al., 2010c; Livingstone et al., 2012; Merritt and Auton, 2000), but these events have not been dated. Radiocarbon dating of marine microfauna indicates an oscillatory ice-margin retreat into northeast Ireland in the period 20.5-16.5 ka BP, approximately coeval with the timing of H1 (McCabe, 2008; McCabe et al., 2007; McCabe et al., 1998). Attempts to correlate readvances across the NISB are hampered by limited dating of events in NW England and on the Isle of Man. Here we provide new geochronological, geophysical and stratigraphical data for the rates and style of deglaciation in the ISB, including multiple new surveys of the seafloor, eleven optically stimulated luminescence (OSL) ages, and eight cosmogenic nuclide surface exposure ages.

This paper: (1) outlines the nature of the glacial sediment/landform imprint relating to the retreat and oscillation of the ISIS; (2) provides chronology to test interpretations that multiple readvances occurred in the NISB during the last deglaciation; (3) explores the synchrony between terrestrial and adjacent marine sectors of the ice mass; and (4) considers the forcing factors controlling ice retreat and readvances.

2.   METHODS

2.1   Terrestrial sites and sampling

The style and timing of deglaciation in the NISB has been discerned from terrestrial evidence for changes in geomorphology, the sediment-landform assemblages and interpreted patterns of ice flow (Knight, 2017; Livingstone et al., 2008, 2010a; Livingstone et al., 2012; McCabe, 2008; Merritt and Auton, 2000; Roberts et al., 2007; Thomas, 1977; Thomas et al., 2006). The ice retreat model is conceptualised here in terms of seven broad zones, with seven boundaries (Fig. 1). Eleven samples for OSL dating from eight sites were targeted at glaciofluvial and deltaic outwash sands associated with well-defined terrestrial ice-marginal positions. Surface exposure dating using in-situ ^{10}Be targeted both glacially-modified bedrock and glacially-faceted and transported boulders in order to provide eight samples from three locations (Fig. 1). A further eight published surface exposure ages (Ballantyne et al., 2013) were recalibrated using a locally-derived ^{10}Be production rate (Fabel et al., 2012). Exposures of the glacial sediments were investigated at coastal sections (Orrisdale, Jurby, Dog Mills and Gutterby), and at the Aldoth, Ballahara and Turkeyland quarries (Fig. 1). Exposures were photographed and logged using field sketches, vertical lithofacies logs and photo-montages following standard procedures (Evans and Benn, 2004; Thomas et al., 2004). The information recorded included textural classification, sedimentary structures, sorting and grain size, palaeo-currents and lithofacies classification. For OSL dating, opaque tubes were hammered into sedimentary sections to prevent exposure to sunlight during sampling and in-situ gamma spectrometry measurements were taken from the tube hole. For surface exposure dating, the rock

3

samples were chiselled from the uppermost boulder and bedrock surfaces. Topographic shielding was measured in the field and corrected for using the CRONUS-Earth online calculator (Balco et al., 2008).

2.2   Offshore geomorphology and geophysics

Unlike other sectors of the ISB, there is a scarcity of palaeoenvironmental data for the waters to the north and east of the Isle of Man. Cruise JC106 of the RRS James Cook (July 2014: Fig. 1) addressed this issue by collecting 380 km of geophysical data and eight cores using the British Geological Survey 6 m vibrocorer and surveying across the seafloor extension of the Bride moraine, east of the Isle of Man (Thomas, 1984). Surveys also extended into the eastern Irish Sea mud-belt (Pantin et al., 1978) and into the deeper waters of the Solway Firth to the north of the Isle of Man (Fig. 1). Geophysical data included multibeam imaging of the seafloor using a Kongsberg EM710 70-100 kHz frequency system, with the data processed using CARIS HIPS. An acoustic stratigraphy was also obtained using a hull-mounted Kongsberg SBP120 sub-bottom profiler (chirp frequency range of 2.5-6.5 kHz). Two-way travel times in seconds were converted to depth below sea level at the time of surveying using typical values of sound velocity (1500 m s^{-1} through the water column and 1600 m s^{-1} through soft sediments). The sub-bottom profiler data were displayed in IHS Kingdom as 2D survey lines. The sediment cores were cut into 1 m long sections, split, photographed and logged recording the sediment shear strength in kPa (Torvane), grain size, sedimentary and deformation structures, colour, sorting, bed contacts, clast abundance and shape and macrofaunal content.

2.3   OSL dating

External beta dose-rates were determined for OSL dating using inductively coupled plasma mass spectrometry (ICP-MS) and inductively coupled plasma atomic emission spectroscopy (ICP-AES), while the external gamma dose-rates were determined using in-situ gamma spectrometry (Table 1). OSL analysis was performed on single grains of quartz. The sample preparation and analysis methods used for OSL dating were identical to those employed by Smedley et al. (2017b). The single-grain D_e values determined for each sample (Fig. 2) are included in the supplementary material (Table S1 - S11). OSL analyses of all samples were performed on grain sizes of 212 – 250 μm, except for sample T3DOGM01 which had a grain size of 150 – 180 μm and so had up to four grains in each hole during single-grain analysis (i.e. microhole analyses). The Finite Mixture Model (FMM) identified four components in the D_e distribution determined for sample T3DOGM01, where the lowest component (0.5 ± 0.2 ka; n = 3 grains) was inconsistent with the geological context of the sample i.e. a 0 Gy dose population that was rejected by applying the screening criteria. However, there was a population of grains that gave an OSL age of 6.0 ± 1.2 ka (n = 4 grains) that was positioned approximately halfway between the 0 Gy dose population and the dominant population. Such populations have previously been suggested to be phantom dose

4

populations caused by averaging the OSL signal from more than one grain during analysis (Arnold and Roberts, 2009). This was probably the case for sample T3DOGM01 as the D_e distribution was determined using microhole measurements rather than single grains; thus, we provide a maximum OSL age for sample T3DOGM01 using the Central Age Model (CAM; 22.5 ± 2.2 ka; Table 2). D_e values were calculated using the Central Age Model (CAM) for D_e distributions that were symmetrical and therefore homogeneously bleached prior to burial, while the minimum age model (MAM) was used to determine D_e values for D_e distributions that were asymmetrically distributed and therefore heterogeneously bleached prior to burial (Table 2). The overdispersion determined from dose-recovery experiments estimated the scatter caused by intrinsic sources of uncertainty that is beyond measurements uncertainties. Intrinsic overdispersion was added in quadrature to the extrinsic scatter arising from external microdosimetry (~20 %) to determine σ_b for the MAM. The CAM or MAM D_e values were divided by the environmental dose-rates to determine an age for each sample (Table 2).

2.4 ^{10}Be surface exposure dating

Eight rock samples were prepared to pure quartz at the University of Glasgow. Quartz was separated from the 250 – 500 µm fraction using standard mineral separation techniques (c.f. Kohl and Nishiizumi, 1992) and purified by ultrasonication in 2 % HF/HNO_3 to remove remaining contaminants and meteoric ^{10}Be. Be extraction was carried out at the Scottish Universities Environmental Research Centre (SUERC), using procedures based on Child et al. (2000). The ^{10}Be/^{9}Be ratios were measured by accelerator mass spectrometry (AMS) at SUERC (Xu et al., 2010) (Table 3). Eight previously published surface exposure ages determined for boulders from Glen Trool (McCarroll et al., 2010) and Gadlach Brae (Ballantyne et al., 2013) in the Galloway Hills of SW Scotland were recalibrated here (Table 4). All new and existing surface exposure ages were calculated using an online calculator (version 2.3 https://hess.ess.washington.edu/; Balco et al., 2008) with time-dependent Lm scaling (Lal, 1991; Stone, 2000) an erosion rate of 1 mm ka^{-1}, and a local production rate, the Loch Lomond production rate (LLPR) which yields a reference sea-level high latitude value of 4.00 ± 0.17 atoms g^{-1} a^{-1} (Fabel et al., 2012) time-dependent Lm scaling. For comparison, the default global production rate in the v2.3 calculator is c. 2.5% higher for our sample locations and yields slightly younger exposure ages (Table 3). Erosion rates on glaciated crystalline rocks are generally quite low at < 2 mm ka^{-1} (André, 2002). Assuming erosion rates of 2 mm ka^{-1} and 0 mm ka^{-1} renders these ages approximately 2% older and 1% younger respectively. Given the small difference in ages our results and interpretation are not sensitive to choice of production rate and/or erosion rates.

2.5   Bayesian age-sequence modelling

The geochronology presented here is distributed across the marginal retreat of the Irish Sea ice stream in the northern ISB. We also discuss parallel ages from higher altitude regions of coastal

5

western Cumbria and the Isle of Man that constrain potentially ice thinning. The geochronological measurements were interrogated using a Bayesian temporal model (Bronk Ramsey, 2009a). This approach provides a basis for identifying data that may be outliers and enables integration of different forms of dating control (exposure and OSL ages). The approach uses the prior order of events (i.e. a prior model) to refine probability distributions when presented as a relative order of events. The prior model is determined independently of the geochronological data. Here the net ice marginal retreat is used as the prior model, ignoring small scale readvances and still-stands of the ice margin. Where a landform is constrained using a single age, there is no method of assessing the influence of geological uncertainties on the accuracy of the age e.g. partial bleaching of the OSL signal or inheritance of the cosmogenic nuclide signal. However, Bayesian analysis uses the prior model, which describes the relationship between depositional events sampled, and the geochronological data to assess the possibility of outliers. Outlier ages identified by this approach are not automatically disregarded; an explanation is sought in terms of the context or the measurement. The approach uses the relationship between sites documenting the northwards passage of the Irish Sea ice margin to restrict the overlapping uncertainty distributions implicit in individual age estimates (Bronk Ramsey 2009a). The Bayesian approach uses the prior model (i.e. the relative order of events) to model the probability distribution of each dating sample and reduces the uncertainty ranges for individual ages because a series of overlapping distributions occur. This modelled chronological framework highlights the timeframe for short-term dynamics of ice margin retreat, such as the oscillations of the ice margin and possible connections to adjacent equivalently modelled sectors of the ice-sheet.

The morpho-stratigraphical model (sensu Chiverrell et al., 2013) for the marginal retreat of Irish Sea ice in the NISB provided the prior model (i.e. hypothetical 'relative-order' of events), which was developed independently of the age information and conceptually underpinned the Bayesian age modelling (Bronk Ramsey, 2009a, b; Buck et al., 1996). The prior model here is complex and integrates the relative distance reconstruction of marginal retreat of Irish Sea ice south to north across the Isle of Man, lowland Cumbria and into southwest Scotland. The surface exposure ages determined for boulders from South Barrule (Isle of Man) and Black Combe (northwest England) represent the timing of ice thinning rather than ice margin retreat, and so were run as outliers (100 %) that do not influence the Bayesian model; this will allow us to explore their relationship to ice thicknesses and surface lowering: ages defined as 100 % outliers in a Bayesian Sequence model do not influence the modelled outputs. Bayesian modelling was completed using OxCal 4.3 and comprised a uniform phase sequence model punctuated by boundaries (see supplemental information). The approach uses Markov chain Monte Carlo (MCMC) sampling to build up a distribution of possible solutions, generating a probability called a posterior density estimate, which is the product of both the prior model and likelihood probabilities for each sample. The approach generated modelled ages for boundaries between seven ice retreat zones (Zone 1 – 7: Fig. 1) and

a final Zone 8 with complete deglaciation. Each retreat zone was coded as a Phase and grouped dating information for sites that share a common relationship with other items in the model. Phases were separated by the Boundary command which delimited each Phase and generated the modelled output of ages (referred to as BL1 to 7: Fig. 1). The sequence model was run in an outlier mode to assess outliers in time using a student's t-distribution (p <0.2) to describe the distribution of outliers using an outlier scaling of $10^{0} – 10^{4}$ years (Bronk Ramsey, 2009b).

3.   RESULTS AND INTERPRETATION

3.1   Coastal lowlands of North Wales (Zone 1)

Zone 1 describes the retreat of ice margins from Anglesey and the Arfon lowlands towards the southern tip of the Isle of Man (Fig. 1). Bedforms from the seafloor between Anglesey and the Isle of Man show east-northeast to west-southwest ice flow directions (Van Landeghem et al., 2009), which suggest an ice margin configuration aligned broadly north-south, and an ice-marginal retreat direction to the northeast. At Aber Ogwen (Edge et al., 1990), coastal exposures show a basal glacial diamict of Welsh provenance overlain by a 2 m thick sequence of laminated sands, silts and clays off-lapping west to east from a diamict high. This lacustrine and deltaic ice-marginal sequence is capped by glacial diamict of Irish Sea affinity. Smedley et al. (2017a) dated two OSL samples which targeted a 0.15 m thick unit of horizontally stratified medium to coarse sand (Sh) above the basal diamict (T4ABER01; 18.1 ± 1.6 ka) and a 0.06 m thick unit of horizontally stratified medium-to-coarse ice proximal bottom-set sands (T4ABER03; 20.2 ± 1.9 ka). These glacigenic sediments on the north Wales coast constrain the decoupling of Irish Sea ice from ice nourished in the mountains of North Wales (BL1: Fig. 1).

3.2   The south of the Isle of Man (Zone 2)

The Plain of Malew (Fig. 3; Roberts et al., 2007; Thomas et al., 2006) records the initial step-back of ice margins in the south of the Isle of Man. Ice flow direction indicators (striae, erratic dispersal trains and glacial bedforms) show an early phase of south-southeast flows over the Southern Manx Uplands followed by a more south-westerly flow associated with bedrock streamlining and drumlins on the Plain of Malew (Fig. 3) (Roberts et al., 2007). River channel diversions on the east coast suggest that coastal areas were occupied by ice longer than the Southern Manx Uplands. This suggests ice thinning on the Isle of Man, but the lack of landforms related to ice-marginal positions and dead ice suggests rapid deglaciation rather than in-situ, ablation-driven downwasting (Roberts et al., 2007). Two surface exposure samples were taken from the upper surface of a roche moutonnée (mid-stoss position), which targeted quartz-rich sandstone (T3CREG01) and a quartz vein in the sandstone (T3CREG02) at ~133 m OD on the Cregneash Peninsula, southwest Isle of Man. The striae in this ice moulded terrain indicate overriding by ice flowing NNW-SSE over the peninsula (Lamplugh, 1903). The surface exposure ages determined for T3CREG01 (21.3 ± 1.2

1 ka) and T3CREG02 (20.9 ± 1.1 ka) are consistent. The low-lying (< 10 m OD) Plain of Malew

2 comprises undulating terrain (< 20 m OD) with drumlins in the east and deglacial outwash sand

3 and gravel plains to the south (Lamplugh, 1898; Lamplugh, 1903; Roberts et al., 2007; Thomas et

4 al., 2004; Thomas et al., 2006). Exposures of these outwash deposits reveal a thin sequence (~2

5 m) of sand and gravel overlying the limestone on the southeast coast (Fig. 3), where a flat-topped

6 outwash terrace yielded horizontally-stratified coarse sands (Sh) with some granular gravel for

7 OSL dating (T3TURK01), which overlies a unit of pebble gravels. The single-grain D_e distribution

8 determined for T3TURK01 was symmetrical (Fig. 2a) and therefore was expected to have been

9 well bleached prior to burial. T3TURK01 was taken from a thin sequence of glacial outwash sand

10 and gravel and therefore probably was deposited in an environment with greater opportunity for

11 sunlight bleaching prior to burial due to transportation in a shallow water column. The CAM age

12 determined for T3TURK01 (19.2 ± 2.0 ka) is consistent with the surface exposure ages determined

13 from Cregneash, and together they constrain the retreat of ice from the south of the Isle of Man

14 (BL2: Fig. 1).

15

16 Samples for surface exposure dating were taken at higher altitudes on South Barrule, the highest

17 peak (483 m) in the Manx Southern Uplands and targeted a train of granite erratic boulders

18 (Darwin, 1848). These erratics were transported ~200 m uphill by ice from bedrock exposures at

19 the head of the Foxdale valley. Sample T3BARR01, from a large (2 x 1.5 x 1 m) rounded quartz-

20 rich granite boulder at 467 m near the summit of South Barrule yielded an exposure age of 25.0 ±

21 1.3 ka (Fig. 4a). Sample T3BARR02, from a smaller (1 x 1 x 1 m) rounded quartz-rich granite

22 boulder at 390 m, produced an exposure age of 18.9 ± 1.0 ka (Fig. 4b). These boulders cannot be

23 linked to specific configurations of the former ice margins, but potentially constrain the timing of ice

24 sheet thinning in the centre of the ISB.

25

3.3 Central Valley of the Isle of Man (Zone 3)

27 The Peel Embayment is located at the western end of the fault-bounded Central Valley of the Isle

28 of Man and contains a complex geomorphology (Fig. 5a) that developed at the lateral margins of

29 western Irish Sea ice (Thomas et al., 2006). Moraine ridges and confined sandar arc south and

30 southwest, and record ice penetration from the west coast of the Isle of Man (Fig. 5a). A small lake

31 (~10 km^2) trapped between the ice margin and the watershed of the Central Valley (at ~50 m OD)

32 facilitated the development of an ice-contact delta. Quarry exposures in this delta at Ballaharra

33 (Fig. 5b) display a sedimentary sequence of ice proximal deltaic sands and gravels (Gt and St),

34 which dip broadly southeast with an ice contact slope immediately to the north (maximum elevation

35 ~50 m). The uppermost 2 m are planar cross-stratified sands and gravels representing a weakly

36 developed delta top-set. Sample T3BALH01 (Fig. 5d) was taken low in the sequence from fine to

37 medium sands (St and Sh) with fine laminations (Fl), which are representative of lower flow

38 conditions in delta toe-sets. Sample T3BALH02 (Fig 5c), from higher in the sequence, was taken

8

from medium to coarse sands (Sr) within planar cross-stratified back-bar gravels (Gp), probably

also deposited during declining river flows on the delta top-set. These OSL ages are age-inverted

with the upper sample being older (T3BALH02; 27.1 ± 3.8 ka) than the lower (T3BALH01; 18.5 ±

3.3 ka). The single-grain D_e distributions for the two samples suggest that the minimum dose

population was characterised better for T3BALH01 than T3BALH02 (Fig. 2b, 2c). This probably

accounts for the age inversion, with T3BALH02 overestimating the true burial age by poorly

constraining the well bleached part of a partially-bleached D_e distribution. This may be explained

by the fact that the coarser-grained T3BALH02 (Sr, Gp) was deposited in a more energetic setting,

potentially with less opportunity for bleaching than the finer-grained suspension rain-out deposits

T3BALH01 (St, Sh, Fl). Thus, the OSL age for T3BALH01 is interpreted as constraining the timing

of this ice margin (BL3: Fig. 1) and the establishment of an ice dammed lake in the Central Valley

(Fig. 5).

3.4   Orrisdale ice marginal oscillations (Zone 4)

The Orrisdale formation is one of three major glacigenic formations (Shellag, Orrisdale and Jurby

Formations) exposed on the northern coastal plain of the Isle of Man (Fig. 6) (Chadwick et al.,

2001; Thomas et al., 2004). The terrain comprises a series of moraine ridges, moraine-confined

sandar and lake basins on the northwest coast. Thomas et al. (1985) divided the thick

accumulations of glaciofluvial outwash deposits (Bishop's Court Member) into: (i) a coarser gravel-

dominated ice proximal lithofacies assemblage (LFA1); and (ii) a finer sand-dominated ice distal

lithofacies assemblage (LFA2). Diamict ridges exposed in coastal cliff sections (Fig. 6; Orrisdale

Head Member) separate the sandur deposits into six adjacent, ice-marginal and parallel troughs.

These features record marginal retreat northwards when ice grounded in the Irish Sea pulled back

from the bedrock core of the Isle of Man. Lapping-off the northernmost ridge structure at Orrisdale

a trough comprising distal sandur deposits (trough 6) of medium-to-fine sands (Sp and Sh) with

ripples (Sr) and fine laminations (Fl) of LFA2 was sampled for OSL dating (T3ORIS01) (Fig. 7A).

Sample T3ORIS01 was taken from Sr lithofacies within the back-bar deposits of planar cross-

stratified sands (Sp). Although the central value of the OSL age for Orrisdale (T3ORIS01; 23.8 ±

3.1 ka) is older than the constraining OSL ages for Ballaharra (central Isle of Man, Zone 3) and

Jurby (northernmost Isle of Man, Zone 5), it lies within uncertainties of these OSL ages and the

minimum dose population in the single-grain D_e distribution appears to be well characterised due to

the large number of D_e values determined for this sample (n = 79 grains; Fig. 2d); thus, it is

considered reliable.

On the east coast of the northern plain, subglacial diamictons associated with the Orrisdale

Formation are restricted to three off-lapping sequences entirely to the north of the Bride Moraine

(Thomas et al., 2004). South of the Bride Moraine, the Dog Mills member consists of laminated,

occasionally massive, fine and silty sands deposited in a proglacial lagoon of lacustrine to shallow

marine nature (Thomas et al., 2004). These horizontally-bedded fine to medium sands (Sh) were sampled for OSL dating (T3DOGM01) (Fig. 6 and 7C). The sampled section was capped by a variable sequence of massive and bedded diamicts (supraglacial massive diamictons), which are intercalated and overlain by sands and gravels (the Kionlough Member) that thin southwards from the Bride Moraine (Thomas et al., 2004). The OSL age for T3DOGM01 could only provide a maximum age for deglaciation at Dog Mills (<22.5 ± 2.2 ka) due to the presence of phantom dose populations discussed previously in the methods, but it is nevertheless consistent with the overall ice-retreat sequence. The Zone 4 ice margin crosses the Isle of Man and extends east towards England, and together the OSL ages from Orrisdale and Dog Mills constrain the timing of ice retreat from BL4 (Fig. 1).

3.5 Southwest Cumbria and northern-most Isle of Man (Zones 5 and 6)

Terrestrial geomorphological data indicate more substantial ice marginal readvances late during the deglaciation of the NISB. Prominent amongst these is the Scottish Readvance, which potentially involved >10 km of ice margin retreat and readvance in northern England (Livingstone et al., 2010c; Merritt and Auton, 2000) and a series of readvances in northeast Ireland, possibly linked with H1 (McCabe et al., 1998). The Scottish Readvance ice margin is postulated to have extended across the lowlands of Cumbria (Fig. 1) and into the eastern ISB down the coast of Cumbria (Livingstone et al., 2010c; Merritt and Auton, 2000; Trotter et al., 1937). It has also been linked (Livingstone et al., 2010c) with a series of readvances north of the Bride Moraine on the Isle of Man (Thomas et al., 2004). The thin geometry of the associated till in the Solway Lowlands (Livingstone et al., 2010d; Trotter and Hollingworth, 1932) and the glaciotectonised succession within the St Bees and Gutterby moraines (Williams et al., 2001) led to suggestions that the Scottish Readvance was a short-lived event. The flow phases and ice-marginal positions are currently based on stratigraphy, rather than geochronological information. Connection of these ice margins across the northeast ISB is uncertain, and so the structure and timing of this readvance episode has yet to be resolved fully. Here we address this with a new geochronology for ice-marginal advances within the Jurby Formation on the Isle of Man (Thomas et al., 2004), the Annaside-Gutterby coastal sections in the southwest Lake District (Huddart, 1977, 1991) and for the Holme St Cuthbert delta complex in lowland Cumbria (Livingstone et al., 2010c).

Jurby, northern Isle of Man: The coastal sections at Jurby on the west coast of the Isle of Man were deposited during a phased 2 – 3 km readvance of the ISIS ice margin into a subaqueous fronting basin (Thomas et al., 2004). The stratigraphy shows four similar off-lapping sediment packages that contain ice contact diamict and subaqueous fan sand-to-mud, grading to distal, laminated muds (Fig. 7B) (Thomas et al., 2004). The Jurby Formation represents a series of readvances of relatively thin ice that extended ~400 – 500 m further than the previous advance, and unconformably overlies the diamictons of the Orrisdale Formation. These advances were

10

followed by rapid retreat during which there was limited erosion or burial of the sediment succession. OSL sampling targeted the second of these sediment packages. The basal sediments are composed of diamict (Orrisdale Head Member) that is unconformably overlain by sands and the massive muds of the Jurby Formation (Thomas et al., 2004). This sequence was then capped by a late glacial kettle hole infill (Fig. 7B). The sampled sands are interpreted as low-energy outwash from subglacial channels evacuating water and sediment either directly or via a short subaerial sandur into open water. OSL samples were taken from a unit of laminated medium to coarse sand (Sh) (T3JURB01) and fine to medium, upward-fining rippled sands (Sh and Sr) (T3JURB02). Both samples were taken from the middle of the cliff section, which is capped by massive muds (Fig. 7B). The OSL ages of 20.8 ± 2.4 ka (T3JURB01) and 23.4 ± 2.8 ka (T3JURB02) overlap within ±1 σ uncertainties, but the central value of the age for T3JURB02 appears to be older. It is more likely that the age determined for sample T3JURB01 is more accurate than T3JURB02 as the D_e distributions for T3JURB01 (Fig. 2j; n = 105 grains) has a larger population of D_e values, which better characterised the minimum dose population in comparison to T3JURB02 (Fig. 2k; n = 83 grains).

Western Lake District: The coastal plain of southwest Cumbria comprises a low <50 m OD undulating terrain of mounds, ridges and basins dissected by outwash channels that formed between the Irish Sea ice mass and Cumbrian Fells (Merritt and Auton, 2000). Samples for surface exposure dating were collected from four glacially-transported boulders of Eskdale granite from 255 m OD) on the western slopes of Black Combe, approximately 2 km east of and 250 m higher than Gutterby-Annaside (Fig. 1). The boulders were originally sourced from the southern margin of a granite outcrop located 3 km to the north of Black Combe, and protrude at least 0.75 m in height above the present ground surface and located within 150 m of one another (Fig. 4C-F). We infer that the suite of boulders was deposited as the ice was downwasting and retreating. Current water depths in the adjacent ISB suggest that ice thicknesses >300 m were required to deposit the boulders on this lateral margin. This therefore corresponded to the lowering of the ice surface during deglaciation. The four samples yielded surface exposure ages of 17.7 ± 1.0, 24.4 ± 1.3, 21.7 ± 1.2 and 22.4 ± 1.3 ka (Table 3), and show significant variation for an individual site. Of these ages, three (T3BC03, 05 and 06) overlap within ± 1σ uncertainties, and provided a weighted mean age of 22.9 ± 1.1 ka that represents the best estimate of the timing of ice surface lowering to ~260 m in the southwest Lake District.

The Annaside-Gutterby complex is composed of north-south aligned ice-marginal ridges that have been associated with readvances of Irish Sea ice down the Cumbrian coastline (Fig. 8). These ridges have been linked with both the Scottish and Gosforth readvances (Huddart, 1977, 1991; Merritt and Auton, 2000), but this has not been supported by any robust chronology. Coastal exposures through the ridges of the Annaside-Gutterby complex show a sequence of glacial

1 diamictons, outwash sands and gravels, and glaciolacustrine sediments (Fig. 8). The basal

2 sediments near Annaside Banks are composed of horizontally-stratified, planar cross stratified and

3 rippled sands (Sh; Sp and Sr) with occasional fine drapes (Fl) that were deposited in a shallow

4 lacustrine setting (Huddart, 1991); these sands were sampled for OSL dating (T3GUTT01). Thick

5 sequences of glaciolacustrine silts/clays interbedded with outwash sands bury these basal sands

6 and reflect a readvance of ice. A second coastal section, 1.2 km to the south of T3GUTT01, also

7 shows lower outwash sands overlain by shallow glaciolacustrine silts/clays with occasional

8 dropstones and these are interbedded with glacifluvial rippled and sub-horizontally bedded sands.

9 These sediments are heavily deformed due to soft sediment deformation suggesting rapid

10 accretion but are also cross-cut by sheared and boudinaged zones related to ice readvance and

11 compressive glaciotectonism of the sediment pile. A clear readvance signal is also supported by

12 the coarsening upwards of glaciofluvial sands and gravels and the emplacement of subglacial

13 diamicts into the upper parts of the glacial sequence. The uppermost 5 – 10 m of the cliff section is

14 composed of massive stratified gravels (Gms) and horizontally stratified and ripped sands (Sh and

15 Sr). An OSL sample (T3GUTT03) was taken from the rippled sands between two gravel units in the

16 upper 3.5 m of the sequence. As a pair of samples, T3GUTT01 provides a constraint on outwash

17 deposition to 27.0 ± 3.3 ka that predated the readvance responsible for the Annaside-Gutterby ice-

18 marginal, glacitectonised complex and sample T3GUTT03 constrains the ultimate retreat of the ice

19 from this ice-marginal ridge to 21.7 ± 2.6 ka (Fig. 8).

20

21 *Holme St Cuthbert (Aldoth Quarry):* The Holme St Cuthbert delta is a 2 km by 4 km lowland (45 m

22 OD) flat-topped ridge composed of sand and gravel, which overlies predominantly NE-SW aligned

23 drumlinised terrain (Fig. 9B) (Livingstone et al., 2008). This superimposition requires that the ice

24 that produced the drumlins must have withdrawn, to be followed by a readvance of ice necessarily

25 from a different direction in order to impound the lake in which the delta accumulated. The delta

26 developed during a late stage south-eastward readvance of ice into the NISB and provides

27 evidence for a lake in the Solway Lowlands dammed by readvance of ice from SW Scotland

28 (Huddart, 1970; Livingstone et al., 2010c), indicating that withdrawal of Cumbrian ice was

29 succeeded by readvance of Scottish ice. During December 2013, the sections at Aldoth Quarry

30 showed the classic components of an ice contact Gilbert-style delta (Fig. 9A), with three broad

31 lithofacies assemblages (LFA1-3). LFA1 is a 5 m thick sequence of sub-horizontal sands and

32 granule gravels, typical of delta-proximal toe-sets, in addition to horizontal muds and sands that

33 were deposited as more distal bottom-sets in a low energy environment (Clemmensen and

34 Houmark-Nielsen, 1981; Cohen, 1979; Gustavson et al., 1975; Jopling and Walker, 1968). LFA2

35 comprises a thick (8 - 9 m) sequence of steeply (30 – 40°) southeast-dipping planar beds of

36 stratified medium-coarse sand with granule to pebble gravels, typical of delta foreset beds

37 deposited as cohesionless subaqueous debris-flows (Nemec, 2009; Nemec et al., 1999; Smith and

38 Ashley, 1985). LFA3 is a ~2 m sequence of glaciofluvial bar-form planar cross-stratified sands and

gravels, rippled sands and massive stratified gravels, interpreted as delta topsets. LFA3 caps the section and was probably deposited by migratory proglacial rivers on the delta surface (Nemec et al., 1999). Sands in the delta top-sets (LFA3) were sampled for OSL dating, specifically from: (i) medium to coarse sand (Sr) from a channel fill (T3ALDO01: Fig 9D); and (ii) a thin (<0.1 m) unit of horizontally stratified coarse sand (Sh) (T3ALDO02) bound by units of coarser outwash sand and gravel (Fig. 9C). These two OSL samples yielded ages of 20.2 ± 3.5 ka (Fig. 2f; T3ALDO01) and 27.9 ± 4.7 ka (Fig. 2g; T3ALDO02). The discrepancy between these two ages probably reflects the different depositional settings of the two samples, whereby T3ALDO01 (Fig. 2f; Fig. 9D) was deposited under lower-energy conditions than T3ALDO02 (Fig. 2g; Fig. 9C), which facilitated a greater opportunity for sunlight exposure prior to burial; thus, the well bleached part of the partially-bleached D_e distribution was characterised using fewer grains.

Offshore stratigraphy: Shallow geophysical and geotechnical data were collected during Cruise JC106 of the RRS James Cook (Fig. 10) and provide information on the environments, continuity of ice marginal positions and relationships in zones 5-6 in the adjacent offshore sector (Fig. 10). The broad stratigraphy and acoustic facies assemblages (AFA1-5; Table 5) are visible in sub-bottom profiler data and corroborated in part by photographs, visual logs and the physical properties from seven vibrocores (Table 5). Retrieved foraminifera from the cores were insufficient in number for ^{14}C dating. Traversing BL5 40 km east of the Isle of Man acoustic survey line x^1-x^2 is parallel to exposures of the glaciotectonic axis of the Bride Moraine at Shellag Point (Fig. 6). Line x^1-x^2 (Fig. 10A) shows a thick basin fill of stratified stronger reflectors probably dense glaciomarine muds (AFA2-4) lapping-off to the north of acoustically more opaque chaotic tectonically-deformed higher terrain (Fig. 10B). The glacigenic sequence AFA1-3 (Fig. 10B) is truncated and buried by less dense Holocene marine sands (AFA4) as confirmed by vibrocore data. The higher terrain in line x^1-x^2 (Fig. 10B) shows a basal opaque and probably dense stratigraphy (AFA1a-d), in which upright structures and lower angle dipping reflectors are similar in character to the diapiric folds and thrusts exposed in coastal sections at Shellag Point (Thomas, 1984). Darker more dense reflectors probably reflect glaciotectonised diamictons (AFA1a), but these are interbedded with less dark units probably coarse and fine grained outwash deposits (AFA1b+d). AFA1a, b and d are all probably similar to components of the glaciotectonised exposures at Shellag Point (Thomas, 1984). In the basin fill (Fig. 10B) extensive folding and deformation of the stratified muds is attributed to a probable readvance of the ice margin and marginal stresses acting against the bedrock slope of the wider Manx platform (Lamplugh, 1903; Pantin et al., 1978). Line x^1-x^2 contains evidence for a more extensive Bride Moraine kinotectonic zone, which formed probably spanning the ice dynamics and marginal readvances attributed to BL4 and BL5 (Fig. 10A). The uppermost undeformed, less dense stratified muds (AFA2) were then deposited under glaciomarine conditions during subsequent ice-marginal retreat, with the lighter reflectors showing stratified Holocene muds (AFA4) capping the sequence.

13

Acoustic line y^1-y^2 (Fig. 10A) extends 7 km from the eastern Irish Sea mud-belt (Pantin et al., 1978) into the Solway Firth (Zone 6) and crosses BL6. Line y^1-y^2 confirms the broad distribution of acoustic facies with a drape of Holocene marine sands and gravels (AFA4) capping darker laminated glaciomarine muds (AFA2-3) that in turn fill an undulating bedrock topography (Fig. 10C). In the south, AFA2-3 are thicker as part of the eastern Irish Sea mud basin (Pantin et al., 1978). Descending into the Solway Firth, the laminated muds (AFA2-3) are restricted to smaller basins between a series of ridges. The ridges are in part acoustically opaque bedrock, but also composed of or capped by darker acoustic units similar to AFA1 as seen on line x^1-x^2 (Fig. 10B). Including examples from at depth in the mud basin, these ridges probably represent a series moraines formed as the ice retreated northwards across BL6. The numerous nature of these ridges (Fig. 10C) appears to reflect still-stand and oscillation of the ice-margin during the retreat of ice margins into Zone 6 (Fig. 10A).

The location of survey line y^2-y^3 was designed to assess the stratigraphy and environments north of BL6 in the middle of Solway Firth (Fig. 10D). The restricted planform multibeam dataset (Fig. 10D) suggest sculpting by subglacial processes that produced moulded and possible drumlinoid forms. The acoustic stratigraphy reveals darker chaotic reflectors at depth (AFA1: Fig. 10D) overlying an acoustically opaque bedrock surface. Relatively thin shelly sands and gravels of Holocene age cap the sequence (AFA4). Vibrocore JC106-084VC confirms that AFA1 includes an over-consolidated Irish Sea-type (Thomas et al., 2004) diamicton (AFA1a: Fig. 11) that is probably interspersed locally with outwash deposits (AFA1b). This is then capped by an overconsolidated laminated glaciomarine mud with numerous drop-stones (AFA1c: Fig. 11) that reflects deglaciation at a calving ice margin and subsequent override by ice readvance. This in turn is overlain by normally-consolidated glaciomarine muds (AFA2) that vibrocore samples suggest are devoid of dropstones (Fig. 11). Both AFA1c and AFA2 contain sparse foraminifera indicative of glaciomarine conditions. The parallel stratified dark reflectors (AFA1c) appear to have been moulded into mounds, for example beneath 084VC and 086VC on line y^2-y^3 (Fig. 10D). The combined sequence of AFA1-3 records the deposition of a subglacial diamicton, followed by ice margin retreat via calving into a marine basin before a readvance consolidated, deformed and moulded the glaciomarine muds into what are probably subglacial bedforms. More extensive multibeam data are required to confirm this, but if the moulded forms are drumlins then the alignment reflects a flow direction 162-158° (SSE) and is consistent with the inferred flow direction of the Scottish Readvance (BL6) (Livingstone et al., 2010d) and possibly later ice marginal oscillations of ice fed from southwest Scotland.

14

3.7 The Galloway Hills, SW Scotland (Zone 7)

During the LGM, the Galloway Hills in SW Scotland formed a major centre of ice dispersal in southern Scotland (Charlesworth, 1927; Geikie, 1894). Ice flowed radially out to the northeast, to the east across northern England, to the northwest and west to Firth of Clyde, and to the south into the Solway Firth, feeding the ISIS (Finlayson, 2013). Eight surface exposure ages have previously been obtained from granite boulders at two sites near the former ice divide: four from Glen Trool (McCarroll et al., 2010) and four from Gadlach Brae (Ballantyne et al., 2013). These ages have been recalibrated here using a locally-derived ^{10}Be production rate (LLPR; Table 4). Two ages (GT-03 and GB-02) represent statistically-distinct outliers, attributed by Ballantyne et al. (2013) to former sediment cover over the sampled boulders. The remaining three samples for Glen Trool (GT-01, GT-2.1 and GT-2.2) produced an uncertainty-weighted mean age of 15.4 ± 0.7 ka, and those for Gadlach Brae yielded an uncertainly-weighted mean age of 15.2 ± 0.8 ka. As these sampled boulders were obtained near the former ice divide, they indicate the timing of deglaciation shortly before the final disappearance of ice from this centre of ice dispersion. These surface exposure ages therefore constrain the ultimate retreat of the ice margin (BL7: Fig. 1) in SW Scotland after deglaciation of the NISB (Zone 6).

3.8 Bayesian age modelling of the deglaciation of the Northern Irish Sea Basin

Bayesian modelling (Bronk Ramsey, 2009a) of the age control for sites recording the northwards retreat of the ISIS margin uses the geochronological measurements and the relative order of events to model the probability distribution of each sample. This process integrates information from multiple dating methods, identifies outliers and uses the series of overlapping distributions to establish posterior density estimates (PDE: 1 σ age ranges italicised below) with smaller uncertainty ranges than the individual age measurements (Bronk Ramsey, 2009a). Boundary limits (BL1 to BL8) inserted within the sequence model also return modelled PDE that provide a temporal framework for the dynamics of ISIS marginal retreat (Table 6). Using these boundary limits to frame understanding of ice marginal dynamics provides a more robust approach than considering the individual age measurements. Surface exposure ages from the uplands of coastal Cumbria and the Isle of Man do not explicitly relate to well defined ISIS marginal positions, and they were excluded from the modelling. They are, however shown in Fig. 12 and Table 6 to explore linkages between the marginal retreat sequence and possible lowering of the ice surface. The Bayesian analysis produced a conformable age model for the ISIS marginal retreat sequence (Fig. 12B, Table 6) with an overall agreement index of 105 % thus exceeding the >60 % threshold advocated by Bronk Ramsey (2009a). Four measurements that potentially constrain ISIS marginal retreat were identified and handled as outliers in the modelling according to uncertainties identified in the prior model or measurement data. At Annaside-Gutterby, OSL sample T3GUTT01 potentially

represents deposits predating the advance of the ISIS to its maximum limits in the Celtic Sea and was excluded from the model. The OSL ages obtained for samples T4BALH02 and T3ALDO02 were, as discussed above, regarded as anomalously old due to poor characterisation of the D_e distribution and treated as 100 % outliers. The recalibrated surface exposure age of sample GB-02, previously regarded as comprised by shielding (Ballantyne et al., 2013) and was handled as a 100 % outlier.

Three other OSL age determinations produce a poor fit to the Bayesian model (A <60%): at Aberogwen (T3ABER01), Orrisdale (T3ORIS01) and Jurby (T3JURB02), with all other age determinations exceeding the 60 % threshold. The agreement indices for these three measurements are A = 46, 57 and 49% respectively, which are close to the A = 60% threshold, but slightly too old relative to the overall Bayesian model. Hence the modelled ages are young relative to the unmodelled age determination. The modelled ages (Table 6) suggest that ice in the NISB retreated 150 – 200 km from the coast of North Wales (BL1: *21.4 ± 1.0 ka*) to the Galloway Hills (BL7: *15.5 ± 0.6 ka*) in ~4 ka. The OSL ages from Aber Ogwen provide the older constraint on the NISB morpho-stratigraphic model (Zone 1). Low altitude sites on the Isle of Man (Cregneash and Turkeyland) constrain the deglaciation of the south of the island (Zone 2), and form the basis for the modelled boundary limit 2 (BL2) of *20.8 ± 0.7 ka*. In the central valley of the Isle of Man, T3BALH02 was rejected as an outlier; thus, T3BALH01 provides the chronological control for the establishment of an ice-dammed lake (Zone 3) constraining BL3 (*20.3 ± 0.7 ka*). The OSL ages for an Orrisdale sandur (T3ORIS01) and Dog Mills proglacial basin (T3DOGM01) constrain the timing of ice margins at the Bride moraine and the Orrisdale Formation (Zone 4) to *19.9 ± 0.7 ka* (BL4). This BL4 age is younger than the age measurements T3ORIS01 and T3DOGM01 but this outcome is guided by the bracketing chronology in Zones 2 and 5/6. Tightly-clustered OSL measurements on feldspars in 45 rock slices obtained from three cobble-sized clasts sampled 1–2 km further south at Orrisdale within Zone 4 have yielded ages of 20.8 ± 1.2, 20.6 ± 0.5 and 21.2 ± 1.2 ka (Jenkins et al., in press), which overlap within uncertainties to the modelled BL4 age of *19.9 ± 0.7 ka*.

Zones 5 and 6 contain more complicated parts of the prior model used in the Bayesian analysis (Fig. 12B), because the precise association and relative order of geochronology from Jurby, Gutterby-Annaside and Holme St Cuthbert (Aldoth) is uncertain. Several iterations of the modelling were undertaken varying the order and grouping of the age information from those three locations (Table 6). For example grouping the chronological data from the three sites as a single Phase, essentially in Oxcal nomenclature an unordered group of ages, produced a conformable (71.7%) Bayesian model (not shown here) with a single boundary age of *18.9 ± 1.0 ka* for Zone 5/6 (Table 6), the Scottish Readvance (Livingstone et al., 2010c). However, a higher agreement index (105 %: Fig. 12B and Table 6) was achieved by grouping Jurby and Gutterby-Annaside (Zone 5) as a

16

1   Phase that predated the dating information from Holme St Cuthbert (Aldoth: Zone 6) (Fig. 12B).

2   This model experiment suggests that Zone 5, constrained by OSL dating at Gutterby-Annaside and

3   Jurby, represents the ice margin (BL5) at *19.3 ± 0.8 ka* and was associated with readvances of 2 –

4   3 km on the Isle of Man. In this model, Zone 6 is constrained by OSL dating at Holme St Cuthbert

5   (Aldoth) and represents an ice margin (BL6) at *18.3 ± 1.1 ka*, providing an alternative age estimate

6   for the Scottish Readvance (Livingstone et al., 2010c). There is very little difference between these

7   two model scenarios: one links the three locations around a boundary age of *18.9 ± 1.0 ka* and the

8   other identifies two boundaries ages that overlap within uncertainties at *19.3 ± 0.8* and *18.3 ± 1.1*

9   *ka*. The offshore sector north of the Isle of Man in the Solway Firth (Zone 6) shows evidence of

10   probable moraines, former ice margins and possible readvances, but failed to yield any dateable

11   materials and so the surface exposure ages from the Galloway Hills in southwest Scotland

12   constrain the ultimate deglaciation of the NISB to before *15.5 ± 0.6 ka* (BL7).

13

4.   DISCUSSION

15   Here we constrain the chronology for ice retreat in the central and eastern sector of the NISB. The

16   new chronology provides timings for a series of readvances of the ice margin, including sites

17   representing the Scottish Readvance limit. It reveals the pace of ice margin retreat in the NISB

18   stepping on to land and into SW Scotland. Bayesian modelling of the geochronology indicates that

19   ice margins retreated in the northern ISB (NISB) along an axial distance of 190 km at an average

20   net rate of 54 m a^{-1} between 21.4 ± 1.0 ka and 15.5 ± 0.6 ka. The distances advanced by the ice

21   margin can in part be assessed, but the precise distances covered during preceding retreat phases

22   is impossible to gauge, thus the distances discussed are net rates. Net ice retreat was faster from

23   the coast of North Wales to the central Isle of Man constrained here at rates of 80 – 180 m a^{-1}, and

24   then slowed to 20 m a^{-1} across the northern Isle of Man (BL3 – 4) before stabilizing at net retreat

25   rates around 15 - 20 m a^{-1} towards the terrestrial hinterlands of southern Scotland. The faster net

26   retreat rates (80 – 180 m a^{-1}) were similar to the faster rates on the northern Llŷn Peninsula where

27   the ice front was less constrained by trough geometry (84 – 139 m a^{-1}) (Smedley et al., 2017a).

28   The slower net retreat rates (13 – 20 m a^{-1}) experienced in the NISB were similar to those

29   reconstructed for the southern Llŷn Peninsula (8–41 m a^{-1}) (Smedley et al., 2017a) and southern

30   Irish coast (26 m a^{-1}) (Small et al., 2018). Slowing of net ice-margin retreat appears to have

31   occurred when the ice was pinned against the bedrock obstruction of the Isle of Man, and was

32   characterised by a series of ice-marginal oscillations within the interval *19.9 ± 0.7* and *18.3 ± 1.1*

33   *ka*; these are recorded in stratigraphical evidence for a series of standstill events and limited

34   (<1km) readvances of the ice margin (Thomas et al., 2004).

35

36   The surface exposure ages obtained for upland settings on the Isle of Man and Cumbria potentially

37   constrain the thinning of ice in the ISB during overall ice-margin retreat. Taken at face value, the

38   boulder surface exposure ages from the Isle of Man suggest ice thinning on the Isle of Man at

1   some time between ~25 and 19 ka to an elevation of 385 m, though it is difficult to assess

2   uncertainties (e.g. nuclide inheritance) using only individual surface exposure ages; thus, this

3   should be treated with some caution. A combined age for the overlapping pair of boulder surface

4   exposure ages at Black Combe constrains ice thinning to 260 m in western Cumbria at 21.5 ± 0.8

5   ka. Assuming that Irish Sea ice was streaming at this time (Van Landeghem et al., 2009) then ice

6   thinning to 385 – 260 m in the NISB and requires the associated ice margins, using typical ice

7   stream surface gradients (0.3 - 0.5°) (Raymond, 2005), to be north of the Llŷn Peninsula. Retreat

8   of ice margins across Llŷn Peninsula have been dated to between 23.9 ±1.6 to 21.1 ± 0.6 ka

9   (Smedley et al., 2017a). The Celtic Sea advance of the ISIS has been suggested to have been a

10   rapid and short-lived event (Chiverrell et al., 2013) and was followed by rapid retreat (Small et al.,

11   2018; Smedley et al., 2017a). Advance and rapid retreat of this nature is likely to have been

12   accompanied by significant drawdown of the ice stream surface and was invoked to explain

13   changes in the retreat of the western lateral margin of the ISIS (Small et al., 2018). The ages for

14   ice thinning in the mountains of the Isle of Man and Cumbria are older than previously published

15   ages in the range 18 – 16 ka for ice free conditions in the Cumbrian Mountains (Ballantyne, 2010;

16   Ballantyne et al., 2009; Wilson and Lord, 2014; Wilson et al., 2013), where a locally-nourished

17   icefield persisted after deglaciation of the NISB. They are fairly similar, however, to surface

18   exposure ages indicating the timing of emergence of higher ground in SE Ireland (~24 – 21 ka), the

19   Wicklow Mountains of eastern Ireland (~22 – 21 ka) and North Wales (~20 – 19 ka) (Ballantyne et

20   al., 2006; Ballantyne and Stone, 2015; Glasser et al., 2012; Hughes et al., 2016).

21

22   The late stage readvances in the Solway Lowlands, Isle of Man and the coastal lowlands of

23   Cumbria were accompanied by realignment of ice flow directions (Livingstone et al., 2010d).

24   Geomorphological and stratigraphical investigations (Livingstone et al., 2010d; Merritt and Auton,

25   2000) have suggested that an ice limit (the Scottish Readvance) that linked the evidence at Jurby,

26   Gutterby-Annaside and Holme St Cuthbert, but hitherto this limit has lacked chronological control.

27   The new OSL and surface exposure ages provided here address this in part by confirming the

28   relationship between ice-marginal positions at these three sites. Given some overlap in the

29   uncertainties for the ages at these three sites, there is synchrony between the Jurby, Gutterby-

30   Annaside and Holme St Cuthbert (Aldoth) positions with boundary limit modelled ages of *19.3 ± 0.8*

31   *ka* (BL5) and *18.3 ± 1.1 ka* (BL6) (Fig. 12A). One solution to the dating evidence from Jurby,

32   Gutterby-Annaside and Holme St Cuthbert (Aldoth) is that they represent a single event dated to

33   *18.9 ± 1.0 ka* thus constraining for the first time the age of the Scottish Readvance. It is equally

34   possible that the deposition of the Holme St Cuthbert delta (Aldoth) and BL6 postdate the Jurby –

35   Gutterby-Annaside cluster with a Boundary Limit age of *18.3 ± 1.1 ka* (BL6), so linking of ice

36   marginal positions between Cumbria and the Isle of Man must remain tentative. On the Isle of Man

37   there is stratigraphical evidence for repeated still-stands and oscillations of the ice margin that

1 range in scale from a few tens of metres at Orrisdale (BL4 to BL5) to more substantial (2 - 3 km)

2 readvances at Jurby and Gutterby-Annaside during decline of the ISIS (Huddart, 1977; Thomas et

3 al., 2004). The stratigraphy at Jurby shows they were each substantial (>1 km) advances of the ice

4 margin within a relatively short period of time (1 – 2 ka) (Thomas et al., 2004). The

5 retreat/readvance distances associated with the Scottish Readvance are impossible to gauge

6 without the degree of coastal exposure that is available at Jurby, and even there the distance of

7 retreat before its subsequent readvance cannot be identified. The proposed timing of the Scottish

8 Readvance (~19.3 – 18.3 ka) is nevertheless interesting with respect to the chronology for ice

9 margin retreat in adjacent regions. South of the Lake District, retreat of ice margins into north

10 Lancashire has been constrained to 18.4 ± 0.8 ka (Chiverrell et al., 2016; Telfer et al., 2009;

11 Wilson et al., 2013). East of the Carlisle Lowlands, the Tyne Gap Ice Stream draining east to the

12 North Sea has a deglacial chronology for the Tyne headwaters that suggests progressive retreat

13 from 18.7 to 17.1 ka (Livingstone et al., 2015). On the Lune and Eden watershed, surface

14 exposure ages from the Shap granite erratic train suggest deglaciation of the Vale of Eden by 17.3

15 ± 0.5 ka (Wilson et al., 2013). Thus, the Scottish Readvance appears to have occurred either

16 slightly before or early during the final deglaciation of much of the eastern Lake District and Tyne

17 Gap.

18

19 The readvances and oscillations in the northeast ISB have been compared previously with the

20 series of ice margin advances recorded on the northeast coast of Ireland (McCabe, 2008). These

21 were constrained by ^{14}C dating of marine microfauna (Ballantyne and Ó Cofaigh, 2017; McCabe,

22 2008) and comprise: (1) deglaciation of the northwest ISB inferred from ice-free conditions at

23 Kilkeel Steps and Cooley Point (Fig.1); (2) the Clogher Head Readvance (radiocarbon dated to

24 ~18.4 ka), constrained by readvance stratigraphical evidence and ages determined for Port, and

25 subsequent retreat ages at Cranfield Point, Linns and Rathcor (Fig. 1); and (3) the Killard Point

26 Readvance, (radiocarbon dated to ~17.3 – 16.6 ka), dated directly at Killard Point (Fig. 1) and

27 bracketed by the ^{14}C dating at Linns and Rathcor and deglacial chronology from Rough Island (Fig.

28 1). This sequence of events forms a logical prior model for the Bayesian modelling of the retreat

29 chronology in northeast Ireland. This model (Fig. 12A) is conformable, contains no outlier ages and

30 produces an overall agreement index of 113 %. The retreat sequence of the northwest ISB (Fig.

31 12A) constrains deglaciation to shortly after *19.8 ± 0.8 ka*, the Clogher Head Readvance to *18.7 ±*

32 *0.2 ka* and the Killard Point Readvance to *17.4 ± 0.3 ka*. Comparing the two Bayesian models (Fig.

33 12) suggests that BL5 at *19.3 ± 0.8 ka* (BL5) broadly corresponds to the Clogher Head Readvance

34 (McCabe, 2008). The Killard Point Readvance at *17.4 ± 0.3 ka* appears to lack an equivalent dated

35 margin in the northeast ISB, but does overlap with the Scottish Readvance (BL6) age range *18.3 ±*

36 *1.1 ka* when Aldoth is treated as a separate Phase in the Bayesian modelling. A series of moraine

37 ridges present on the seafloor of the Solway Firth are also potentially equivalent to the Killard Point

38 Readvance moraine, but currently lack dating control. Contrasting the western and eastern sectors

of the NISB, the deeper western basin was clearly deglaciated earlier. In the eastern ISB the deglaciation appears to be topographically controlled with retreat rate a function of the extent of the calving margin and the ice margin displayed oscillatory behaviour against the pinning point of the Isle of Man. If this behaviour is independent of regional forcing, perhaps similar dynamics in the western ISB reflect the transition from a calving margin approaching the coast of Ireland.

Comparing the dynamics of ice retreat in the ISB with forcing or conditioning factors (Fig. 13) shows a broad match between retreat and increasing summer insolation (Berger and Loutre, 1991). Following the short-lived advance of the ISIS into the Celtic Sea, overall ice-marginal retreat in the southern ISB that was punctuated by still-stands and oscillations, recorded from south to north along the coastlines of Ireland and Wales (Small et al., 2018; Smedley et al., 2017a). Faster (e.g. 84 - 118 m a^{-1}) and shorter-lived phases of retreat (over centennial timeframes) occurred across the Llŷn Peninsula during periods of relatively stable climate driven by internal dynamics as the ISIS experienced a widening of the calving margin and a deepening of the trough (Smedley et al., 2017a). The new data presented here, suggests that calving margin width continued to produce faster retreat rates (80 - 180 m a^{-1}) from North Wales (BL1: 21.2 ± 1.0 ka) to the Central Valley of the Isle of Man (BL2: 20.7 ± 0.7 ka), at a time when external forcing factors (e.g. climate, relative sea level and sea surface temperatures) were relatively stable (Fig. 13). The calving width then narrowed as the ISIS wrapped around the Isle of Man. This phase corresponded to a reduction in net margin retreat rate in the interval from 20.3 ± 0.7 ka (BL3) to 19.3 ± 0.8 ka (BL5), with evidence for at least ten ice-marginal oscillations (Thomas et al., 2004) in relatively quick succession (within 1 ka) as sectors on and to the east of Isle of Man developed a terrestrially-terminating ice margin. These still-stands and readvances (BL5-6) are similar in character to the centennial-scale oscillations recorded on the Llŷn Peninsula (Smedley et al., 2017a). This period of ice stability coincided with both stable climatic and oceanic conditions (Fig. 13) and the later stages of ice thinning in the mountains of the Isle of Man and North Wales (Hughes et al., 2016). Lake District and southern Ireland (Ballantyne and Stone, 2015). The ice front then retreated from the NISB and towards SW Scotland as air temperatures north of ~45 °N warmed in response to increasing summer insolation (Fig. 13). The responses of ice in this northeast sector of the ISB during H1 at ~ 17.4 ka may be reflected in BL6, but also in the form of moraine ridges on the seafloor north of the Isle of Man, but these landforms remain undated.

Overall, the new chronology presented here suggests that ice-marginal retreat in the NISB was driven by a loss or reduction of a calving margin as the ice front became pinned by the Isle of Man. The numerous and substantial ice-marginal oscillations experienced prior to this were probably driven by internal readjustments of the ice mass, which emphasises the importance of hypsometry on ice margin stability and oscillations. Once the air temperatures north of ~45 °N began to

increase substantially in response to summer insolation (Fig. 13) (Bintanja et al., 2005) ice margins retreated from the ISB and into southwest Scotland.

5.   CONCLUSIONS

The retreat of the ISIS in the northern ISB was more rapid (80 to 180 m a^{-1}) in southern sectors when ice margins retreated northwards from the Llŷn Peninsula to the Central Valley on the Isle of Man at ca. 20 ka. Average retreat rates then slowed to 13 – 20 m a^{-1} when the ice margin oscillated northwards across the northern Isle of Man and lowland Cumbria and experienced both limited and large-scale (>1 – 2 km) retreat-readvance cycles before retreating northwards into the Galloway Hills in southwest Scotland. Surface exposure ages obtained for high ground on the Isle of Man (18.9 ± 1.0 ka) and western Cumbrian Mountains (21.5 ± 0.8 ka) overlap with the rapid retreat of ice from maximum limits in the Celtic Sea (Praeg et al., 2015; Smedley et al., 2017b) with ice margins retreating across the Llŷn Peninsula from 23.9 ±1.6 to 21.1 ± 0.6 ka (Smedley et al., 2017a) and the Isle of Man from 20.8 ±0.7 to 18.3 ka. The rapid advance of the ISIS to and subsequent retreat from maximum limits when associated with unambiguous evidence for ice streaming in the central ISB (Van Landeghem et al., 2009) provides a context for significant drawdown of the ice stream surface.

New ages from multiple positions along ice limits (Livingstone et al., 2010) attributed to the Scottish Readvance (Trotter et al., 1937) constrain it to the period *19.3 ± 0.8* to *18.3 ± 1.1 ka*. The evidence for >1 – 2 km readvances of the ice margin at Jurby, Gutterby-Annaside and Holme St Cuthbert (Aldoth) is unequivocal (Huddart, 1977; Livingstone et al., 2010c; Thomas et al., 2004), but was accompanied by numerous other smaller scale oscillations and standstills of the ice margin, for example those elsewhere on the Cumbrian coast (Trotter et al., 1937) and those within the Orrisdale complex on the Isle of Man (Thomas et al., 2004). The new chronology suggests that it is possible that the Scottish Readvance was a regionally penecontemporaneous event in the Cumbrian lowlands and the northern Isle of Man, and predated advance limits (possibly linked with H1) in the north of Ireland. Our chronology provides no evidence for ice margin readvances synchronous with H1, but may be reflected in ridges shown in geophysical data from the sea floor north of the Scottish Readvance limit in the Solway Firth.

Over-printing a general retreat sequence probably driven by increased summer insolation, there are variations in ice retreat rates in the NISB that support suggestions that internal ice dynamics responding to a wider calving margin and deeper trough coincide with faster ice retreat. The feasibility of the timing and scale of marginal oscillations during deglaciation in response to internal and external forcing could be tested using ice sheet modelling experiments. The slowing of ice-marginal retreat across the Isle of Man coincided with a reduced calving front, a normal bedslope and a pinning point, in addition to the development of a terrestrially-terminating ice margin.

21

Comparison of the regional ice retreat chronologies show that as ice marginal retreat slowed around the Isle of Man, there was a regional asynchrony as the deeper western ISB had deglaciated more rapidly and completely. Retreat and readvance dynamics near the present coast of eastern Ireland in the interval 20 – 18 ka could also represent a response to a transition from an extensive calving margin. Ultimately, the rapid deglaciation of the NISB from the Solway Firth into the Galloway Hills coincided with climate warming, driven by increased summer insolation. Overall, this new retreat sequence highlights the importance of internal dynamics in controlling ice retreat rates in the Irish Sea, but also documents the final demise of the ice in the NISB which occurs at the same time as climate warming north of ~45 °N.

ACKNOWLEDGEMENTS

REFERENCES

André, M.F. (2002) Rates of Postglacial rock weathering on glacially scoured outcrops (Abisko-Riksgränsen area, 68°N). Geografiska Annaler, Series A: Physical Geography 84, 139-150.

Arnold, L.J., Roberts, R.G. (2009) Stochastic modelling of multi-grain equivalent dose (De) distributions: Implications for OSL dating of sediment mixtures. Quaternary Geochronology 4, 204-230.

Balco, G., Stone, J.O., Lifton, N.A., Dunai, T.J. (2008) A complete and easily accessible means of calculating surface exposure ages or erosion rates from 10Be and 26Al measurements. Quaternary Geochronology 3, 174-195.

Ballantyne, C.K. (2010) Extent and deglacial chronology of the last British-Irish Ice Sheet: Implications of exposure dating using cosmogenic isotopes. Journal of Quaternary Science 25, 515-534.

Ballantyne, C.K., McCarroll, D., Stone, J.O. (2006) Vertical dimensions and age of the Wicklow Mountains ice dome, Eastern Ireland, and implications for the extent of the last Irish Ice Sheet. Quaternary Science Reviews 25, 2048-2058.

Ballantyne, C.K., Ó Cofaigh, C., (2017) The last Irish Ice Sheet: extent and chronology, Advances in Irish Quaternary Studies. Springer, pp. 101-149.

Ballantyne, C.K., Rinterknecht, V., Gheorghiu, D.M. (2013) Deglaciation chronology of the Galloway Hills Ice Centre, southwest Scotland. Journal of Quaternary Science 28, 412-420.

Ballantyne, C.K., Stone, J.O. (2015) Trimlines, blockfields and the vertical extent of the last ice sheet in Southern Ireland. Boreas 44, 277-287.

Ballantyne, C.K., Stone, J.O., Fifield, L.K. (2009) Glaciation and deglaciation of the SW Lake District, England: implications of cosmogenic 36Cl exposure dating. Proceedings of the Geologists' Association 120, 139-144.

Bard, E. (2002) Climate shock: Abrupt changes over millennial time scales. Physics Today 55, 32-38.

Bard, E., Rostek, F., Hénot-Combes, G. (2004) A Better Radiocarbon Clock. Science 303, 178-179.

Berger, A., Loutre, M.F. (1991) Insolation values for the climate of the last 10 million years. Quaternary Science Reviews 10, 297-317.

Bintanja, R., van de Wal, R.S.W., Oerlemans, J. (2005) Modelled atmospheric temperatures and global sea levels over the past million years. Nature 437, 125-128.

Bond, G., Heinrich, H., Broecker, W., Labeyrie, L., McManus, J., Andrews, J., Huon, S., Jantschik, R., Clasen, S., Simet, C., Tedesco, K., Klas, M., Bonani, G., Ivy, S. (1992) Evidence for massive discharges of icebergs into the North Atlantic ocean during the last glacial period. Nature 360, 245-249.

1 Bradley, S.L., Milne, G.A., Shennan, I., Edwards, R. (2011) An improved glacial isostatic
2 adjustment model for the British Isles. Journal of Quaternary Science 26, 541-552.

3 Bronk Ramsey, C. (2009a) Bayesian analysis of radiocarbon dates. Radiocarbon 51, 337-360.

4 Bronk Ramsey, C. (2009b) Dealing with outliers and offsets in radiocarbon dating. Radiocarbon 51,
5 1023-1045.

6 Buck, C.E., Cavanagh, W.G., Litton, C.D. (1996) Bayesian Approach to Interpreting Archaeological
7 Data.

8 Chadwick, R.A., Jackson, D.I., Barnes, R.P., Kimbell, G.S., Johnson, H., Chiverrell, R.C., Thomas,
9 G.S.P., Jones, N.S., Riley, N.J., Pickett, E.A., Young, B., Holliday, D.W., Ball, D.F., Molyneux,
10 S.G., Long, D., Power, G.M., Roberts, D.H. (2001) Geology of the Isle of Man and its offshore
11 area. British Geological Survey Research Report.

12 Child, D., Elliott, G., Mifsud, C., Smith, A.M., Fink, D. (2000) Sample processing for earth science
13 studies at ANTARES. Nuclear Instruments and Methods in Physics Research, Section B: Beam
14 Interactions with Materials and Atoms 172, 856-860.

15 Chiverrell, R.C., Burke, M.J., Thomas, G.S.P. (2016) Morphological and sedimentary responses to
16 ice mass interaction during the last deglaciation. Journal of Quaternary Science 31, 265-280.

17 Chiverrell, R.C., Thrasher, I.M., Thomas, G.S.P., Lang, A., Scourse, J.D., van Landeghem, K.J.J.,
18 McCarroll, D., Clark, C.D., Ó'Cofaigh, C., Evans, D.J.A., Ballantyne, C.K. (2013) Bayesian
19 modelling the retreat of the Irish Sea Ice Stream. Journal of Quaternary Science 28, 200-209.

20 Clemmensen, L.B., Houmark-Nielsen, M. (1981) Sedimentary features of a Weichselian
21 glaciolacustrine delta. Boreas 10, 229-245.

22 Cohen, J.M. (1979) Deltaic sedimentation in glacial lake Blessington, County Wicklow, Ireland.
23 Proc. INQUA symposium on genesis and lithology of Quaternary deposits, Zurich, 10-20
24 September 1978. Moraines and varves: origin, genesis, classification, 357-368.

25 Darwin, C. (1848) On the transportal of erratic boulders from a lower to a higher level. Quarterly
26 Journal of the Geological Society of London 4, 315-323.

27 Durcan, J.A., King, G.E., Duller, G.A.T. (2015) DRAC: Dose Rate and Age Calculator for trapped
28 charge dating. Quaternary Geochronology 28, 54-61.

29 Edge, M.J., Hart, J., Pointon, K., (1990) The sequences at Aber Ogwen and Glan-y-mor-isaf, in:
30 Addison, K., Edge, M.J., Watkins, R. (Eds.), The Quaternary of North Wales: Field Guide.
31 Quaternary Research Association, Coventry, pp. 119-130.

32 Evans, D.J.A., Benn, D.I. (2004) A Practical Guide to the Study of Glacial Sediments. A Practical
33 Guide to the Study of Glacial Sediments.

34 Fabel, D., Ballantyne, C.K., Xu, S. (2012) Trimlines, blockfields, mountain-top erratics and the
35 vertical dimensions of the last British-Irish Ice Sheet in NW Scotland. Quaternary Science Reviews
36 55, 91-102.

1　Glasser, N.F., Hughes, P.D., Fenton, C., Schnabel, C., Rother, H. (2012) 10Be and 26Al exposure-
2　age dating of bedrock surfaces on the Aran ridge, Wales: evidence for a thick Welsh Ice Cap at the
3　Last Glacial Maximum. Journal of Quaternary Science 27, 97-104.

4　Guérin, G., Mercier, N., Adamiec, G. (2011) Dose-rate conversion factors: update. Ancient TL 29,
5　5-8.

6　Guérin, G., Mercier, N., Nathan, R., Adamiec, G., Lefrais, Y. (2012) On the use of the infinite matrix
7　assumption and associated concepts: A critical review. Radiation Measurements 47, 778-785.

8　Gustavson, T.C., Ashley, G.M., Boothroyd, J.C. (1975) Depositional sequences in glaciolacustrine
9　deltas. Glaciofluvial and Glaciolacustrine Sedimentation 23, 264-280.

10　Haapaniemi, A.I., Scourse, J.D., Peck, V.L., Kennedy, H., Kennedy, P., Hemming, S.R., Furze,
11　M.F.A., Pienkowski, A.J., Austin, W.E.N., Walden, J., Wadsworth, E., Hall, I.R. (2010) Source,
12　timing, frequency and flux of ice-rafted detritus to the Northeast Atlantic margin, 30-12 ka: Testing
13　the Heinrich precursor hypothesis. Boreas 39, 576-591.

14　Huddart, D. (1970) Aspects of Glacial Sedimentation in the Cumberland Lowland. Aspects of
15　Glacial Sedimentation in the Cumberland Lowland.

16　Huddart, D. (1971) A relative glacial chronology from the tills of the Cumberland lowland.
17　Proceedings of the Cumberland Geological Society 3, 21-32.

18　Huddart, D. (1977) Gutterby Spa - Annaside Banks Moraine and St. Bees Moraine. The Isle of
19　Man, Lancashire Coast and Lake District.

20　Huddart, D., (1991) The glacial history and glacial deposits of the north and west Cumbrian
21　lowlands, in: Ehlers, J., Gibbard, P.L., Rose, J. (Eds.), Glacial deposits of Great Britain and Ireland.
22　Balkema, Rotterdam. Balkema, Rotterdam, pp. 151-167.

23　Huddart, D., Glasser, N.F. (2002) Quaternary of Northern England. GCR Series 25, 745.

24　Hughes, P.D., Glasser, N.F., Fink, D. (2016) Rapid thinning of the Welsh Ice Cap at 20–19ka
25　based on 10Be ages. Quaternary Research 85, 107-117.

26　Jackson, D.I., Jackson, A.A., Evans, D., Wingfield, R.T.R., Barnes, R.P., Arthur, M.J. (1995) United
27　Kingdom Offshore Regional Report: The Geology of the Irish Sea.

28　Jopling, A.V., Walker, R.G. (1968) Morphology and origin of ripple-drift cross-lamination, with
29　examples from the Pleistocene of Massachusetts. Journal of Sedimentary Petrology 38, 971-984.

30　Knight, J., (2017) Deglaciation of the Northern Irish Sea Basin, in: Coxon, P., McCarron, S.,
31　Mitchell, F. (Eds.), Advances in Irish Quaternary Studies. Atlantis Press, Paris, pp. 151-180.

32　Kohl, C.P., Nishiizumi, K. (1992) Chemical isolation of quartz for measurement of in-situ -produced
33　cosmogenic nuclides. Geochimica et Cosmochimica Acta 56, 3583-3587.

34　Lal, D. (1991) Cosmic ray labeling of erosion surfaces: in situ nuclide production rates and erosion
35　models. Earth and Planetary Science Letters 104, 424-439.

Lamplugh, G.W., (1898) Geological Survey of England and Wales. Isle of Man. Geologically surveyed by G.W. Lamplugh 1892-97 ... Scale of one inch to a statute mile. Ordnance Survey Office, Southampton.

Lamplugh, G.W. (1903) The geology of the Isle of Man. Memoir of the Geological Survey of the United Kingdom.

Lawrence, K.T., Herbert, T.D., Brown, C.M., Raymo, M.E., Haywood, A.M. (2009) High-amplitude variations in north atlantic sea surface temperature during the early pliocene warm period. Paleoceanography 24.

Livingstone, S.J., Cofaigh, C.Ó., Evans, D.J.A. (2008) Glacial geomorphology of the central sector of the last British-Irish Ice sheet. Journal of Maps 4, 358-377.

Livingstone, S.J., Cofaigh, C.Ó., Evans, D.J.A. (2010a) A major ice drainage pathway of the last British-Irish ice sheet: The Tyne Gap, Northern England. Journal of Quaternary Science 25, 354-370.

Livingstone, S.J., Evans, D.J.A., Cofaigh, C.Ó., Hopkins, J. (2010b) The Brampton kame belt and Pennine escarpment meltwater channel system (Cumbria, UK): Morphology, sedimentology and formation. Proceedings of the Geologists' Association 121, 423-443.

Livingstone, S.J., Evans, D.J.A., Ó'Cofaigh, C. (2010c) Re-advance of Scottish ice into the Solway Lowlands (Cumbria, UK) during the Main Late Devensian deglaciation. Quaternary Science Reviews 29, 2544-2570.

Livingstone, S.J., Evans, D.J.A., Ó'Cofaigh, C., Davies, B.J., Merritt, J.W., Huddart, D., Mitchell, W.A., Roberts, D.H., Yorke, L. (2012) Glaciodynamics of the central sector of the last British-Irish Ice Sheet in Northern England. Earth-Science Reviews 111, 25-55.

Livingstone, S.J., Ó'Cofaigh, C., Evans, D.J., Palmer, A. (2010d) Sedimentary evidence for a major glacial oscillation and proglacial lake formation in the Solway Lowlands (Cumbria, UK) during Late Devensian deglaciation. Boreas 39, 505-527.

Livingstone, S.J., Roberts, D.H., Davies, B.J., Evans, D.J.A., Ó Cofaigh, C., Gheorghiu, D.M. (2015) Late Devensian deglaciation of the Tyne Gap Palaeo-Ice Stream, northern England. Journal of Quaternary Science 30, 790-804.

McCabe, A.M. (2008) Glacial geology and geomorphology: the landscapes of Ireland. Dunedin Academic Press, Edinburgh.

McCabe, A.M., Clark, P.U., Clark, J., Dunlop, P. (2007) Radiocarbon constraints on readvances of the British–Irish Ice Sheet in the northern Irish Sea Basin during the last deglaciation. Quaternary Science Reviews 26, 1204-1211.

McCabe, A.M., Knight, J., McCarron, S. (1998) Evidence for Heinrich event 1 in the British Isles. Journal of Quaternary Science 13, 549-568.

McCarroll, D., Stone, J.O., Ballantyne, C.K., Scourse, J.D., Fifield, L.K., Evans, D.J.A., Hiemstra, J.F. (2010) Exposure-age constraints on the extent, timing and rate of retreat of the last Irish Sea ice stream. Quaternary Science Reviews 29, 1844-1852.

26

1   Merritt, J.W., Auton, C.A., (2000) An outline of the lithostratigraphy and depositional history of Quaternary deposits in the Sellafield district, west Cumbria, Proceedings of the Yorkshire Geological and Polytechnic Society. Geological Society of London, pp. 129-154.

4   Nemec, W., (2009) Aspects of Sediment Movement on Steep Delta Slopes, Coarse-Grained Deltas, pp. 29-73.

6   Nemec, W., Lønne, I., Blikra, L.H. (1999) The Kregnes moraine in Gauldalen, west-central Norway: Anatomy of a Younger Dryas proglacial delta in a palaeofjord basin. Boreas 28, 454-476.

8   Pantin, H.M., Hughes, M.J., Wilson, J.B. (1978) Quaternary sediments from the north-east Irish Sea: Isle of Man to Cumbria. Bulletin of the Geological Survey of Great Britain 64, 1-43.

10   Praeg, D., McCarron, S., Dove, D., Cofaigh, C.O., Scott, G., Monteys, X., Facchin, L., Romeo, R., Coxon, P. (2015) Ice sheet extension to the Celtic Sea shelf edge at the Last Glacial Maximum. Quaternary Science Reviews 111, 107-112.

13   Prescott, J.R., Hutton, J.T. (1994) Cosmic ray contributions to dose rates for luminescence and ESR dating: Large depths and long-term time variations. Radiation Measurements 23, 497-500.

15   Rasmussen, S.O., Bigler, M., Blockley, S.P., Blunier, T., Buchardt, S.L., Clausen, H.B., Cvijanovic, I., Dahl-Jensen, D., Johnsen, S.J., Fischer, H., Gkinis, V., Guillevic, M., Hoek, W.Z., Lowe, J.J., Pedro, J.B., Popp, T., Seierstad, I.K., Steffensen, J.P., Svensson, A.M., Vallelonga, P., Vinther, B.M., Walker, M.J.C., Wheatley, J.J., Winstrup, M. (2014) A stratigraphic framework for abrupt climatic changes during the Last Glacial period based on three synchronized Greenland ice-core records: Refining and extending the INTIMATE event stratigraphy. Quaternary Science Reviews 106, 14-28.

22   Raymond, M.J. (2005) On the relationship between surface and basal properties on glaciers, ice sheets, and ice streams. Journal of Geophysical Research 110.

24   Roberts, D.H., Dackombe, R.V., Thomas, G.S.P. (2007) Palaeo-ice streaming in the central sector of the British-Irish Ice Sheet during the Last Glacial Maximum: evidence from the northern Irish Sea Basin. Boreas 36, 115-129.

27   Small, D., Smedley, R.K., Chiverrell, R.C., Scourse, J.D., Ó Cofaigh, C., Duller, G.A.T., McCarron, S., Burke, M.J., Evans, D.J.A., Fabel, D., Gheorghiu, D.M., Thomas, G.S.P., Xu, S., Clark, C.D. (2018) Trough geometry was a greater influence than climate-ocean forcing in regulating retreat of the marine-based Irish-Sea Ice Stream. Geological Society America Bulletin.

31   Smedley, R.K., Chiverrell, R.C., Ballantyne, C.K., Burke, M.J., Clark, C.D., Duller, G.A.T., Fabel, D., McCarroll, D., Scourse, J.D., Small, D., Thomas, G.S.P. (2017a) Internal dynamics condition centennial-scale oscillations in marinebased ice-stream retreat. Geology 45, 787-790.

34   Smedley, R.K., Scourse, J.D., Small, D., Hiemstra, J.F., Duller, G.A.T., Bateman, M.D., Burke, M.J., Chiverrell, R.C., Clark, C.D., Davies, S.M., Fabel, D., Gheorghiu, D.M., McCarroll, D., Medialdea, A., Xu, S. (2017b) New age constraints for the limit of the British–Irish Ice Sheet on the Isles of Scilly. Journal of Quaternary Science 32, 48-62.

38   Smith, N.D., Ashley, G.M. (1985) Proglacial lacustrine environment. Glacial sedimentary environments, 135-216.

27

1 Stone, J.O. (2000) Air pressure and cosmogenic isotope production. Journal of Geophysical
2 Research: Solid Earth 105, 23753-23759.

3 Telfer, M.W., Wilson, P., Lord, T.C., Vincent, P.J. (2009) New constraints on the age of the last ice
4 sheet glaciation in NW England using optically stimulated luminescence dating. Journal of
5 Quaternary Science 24, 906-915.

6 Thomas, G.S.P., (1977) The quaternary of the Isle of Man, in: Tooley, M.J. (Ed.), The Quaternary
7 history of the Irish Sea. Steel House Press, Liverpool. Geological Journal Special Issue, pp. 155-
8 178.

9 Thomas, G.S.P. (1984) The origin of the glacio-dynamic structure of the Bride Moraine, Isle of
10 Man. Boreas 13, 355-364.

11 Thomas, G.S.P., Chiverrell, R., Huddart, D. (2004) Ice-marginal depositional responses to
12 readvance episodes in the Late Devensian deglaciation of the Isle of Man. Quaternary Science
13 Reviews 23, 85-106.

14 Thomas, G.S.P., Chiverrell, R.C., Huddart, D., Long, D., Roberts, D.H., (2006) The Ice Age, in:
15 Chiverrell, R.C., Thomas, G.S.P. (Eds.), A New History of the Isle of Man: Volume 1 Evolution of
16 the natural landscape. Liverpool University Press, Liverpool, pp. 126-219.

17 Thomas, G.S.P., Connaughton, M., Dackombe, R.V. (1985) Facies Variation in a Late Pleistocene
18 Supraglacial Outwash Sandur from the Isle-of-Man. Geological Journal 20, 193-213.

19 Trotter, F.M., Hollingworth, S.E. (1932) The Glacial Sequence in the North of England. Geological
20 Magazine 69, 374-380.

21 Trotter, F.M., Hollingworth, S.E., Eastwood, T., Rose, W.C.C. (1937) Gosforth District. Geological
22 Survey Memoir, England and Wales, Sheet 37.

23 Van Landeghem, K.J.J., Wheeler, A.J., Mitchell, N.C. (2009) Seafloor evidence for palaeo-ice
24 streaming and calving of the grounded Irish Sea Ice Stream: Implications for the interpretation of its
25 final deglaciation phase. Boreas 38, 111-131.

26 Williams, G.D., Brabham, P.J., Eaton, G.P., Harris, C. (2001) Late Devensian glaciotectonic
27 deformation at St Bees, Cumbria: a critical wedge model. Journal of the Geological Society 158,
28 125-135.

29 Wilson, P., Lord, T. (2014) Towards a robust deglacial chronology for the northwest England sector
30 of the last British-Irish Ice Sheet. North West Geography 14.

31 Wilson, P., Lord, T., Rodés, Á. (2013) Deglaciation of the eastern Cumbria glaciokarst, northwest
32 England, as determined by cosmogenic nuclide (10Be) surface exposure dating, and the pattern
33 and significance of subsequent environmental changes. Cave and Karst Science 40, 22-27.

34 Xu, S., Dougans, A.B., Freeman, S.P.H.T., Schnabel, C., Wilcken, K.M. (2010) Improved 10Be and
35 26Al-AMS with a 5 MV spectrometer. Nuclear Instruments and Methods in Physics Research,
36 Section B: Beam Interactions with Materials and Atoms 268, 736-738.

1

2 1   **Table and Figure captions**

3 2   Fig. 1. Location and context of the northern Irish Sea Basin plotted on Nextmap™ and EMODnet
4 3   topographical data (http://www.emodnet-hydrography.eu/). This shows inferred ice margins (red
5 4   and white) including the possible extent of the calving margins. Triangles denote cores and
6 5   geophysical survey lines (black dashed lines) taken on the cruise JC106 and the locations of
7 6   dating sites. The zones (1-7) and boundaries (BL1 to 7) used the chronological model are
8 7   identified.
9
10

11 8   Fig. 2. Abanico plots of the D_e values determined for OSL dating. Note that sample T3DOGM01
12 9   was analysed using microhole analyses (i.e. up to four grains in each hole due to a grain size of
13 10   150 – 180 µm) rather than single grains and so the CAM provides a maximum OSL age for this
14 11   sample. The abanico plots shown present the D_e distributions in two plots that share a common z-
15 12   axis of D_e values: (1) a bivariate plot where each D_e value is presented in relation to its precision
16 13   (shown on the x-axis, where those more precisely known have greater values of precision); this is
17 14   similar to the radial plot commonly used in luminescence dating; and (2) a univariate plot showing
18 15   the age frequency distribution of D_e values, which does not give any presentation of the precision
19 16   of individual D_e values. The grey shading across both plots shows the CAM or MAM D_e for each
20 17   distribution (± 2 σ shown on the y-axis). The combination of these two plots aids interpretation of
21 18   the scatter in the D_e distributions, where samples with a greater range of D_e values on the z-axis
22 19   have larger amounts of scatter in the D_e distribution.
23
24

25 20   Fig. 3. Glacial geomorphology of the south of the Isle of Man and a 5 km Ordnance Survey grid
26 21   (Roberts et al., 2007; Thomas et al., 2006) showing the locations of samples T3CREG01 and
27 22   T3CREG02, T3TURK01 and T3BARR01 and T3BARR02.
28
29

30 23   Fig. 4. Cosmogenic nuclide samples: A. T3BARR01 from the summit of South Barrule, B.
31 24   T3BARR02 from the flanks of South Barrule on the Isle of Man. C-F. Samples T3BC02, T3BC03,
32 25   T3BC05 and T3BC06 from Black Combe in western Cumbria, NW England.
33
34

35 26   Fig. 5. A. Glacial geomorphology of the Peel Embayment, central Isle of Man (after Thomas et al.,
36 27   2006) and a 1 km Ordnance Survey grid, showing the locations of samples T3BALH01 and
37 28   T3BALH02. B. Quarry section photographs, summary stratigraphy and lithofacies at Ballaharra
38 29   quarry on 7/11/2013, and samples C. T3BALH01 and D. T3BALH02.
39
40

41 30   Fig. 6. Lithostratigraphy of the Northern Plain of the Isle of Man (after Thomas et al., 2004; Thomas
42 31   et al., 2006) with a 5 km Ordnance Survey grid. Summary stratigraphy and lithofacies assemblages
43 32   on the east and west coasts of the Northern Plain of the Isle of Man, identifying the OSL sample
44 33   locations from Orrisdale (T3ORIS01), Dog Mills (T3DOGM01) and Jurby (T3JURB01, T3JURB02).
45 34   Stratigraphical sections show the three major glacigenic formations (from oldest to youngest: the
46 35   Shellag, Orrisdale and Jurby Formations). Stratigraphic units comprise in the Shellag Formation:
47 36   S1 basal diamict; S2 ice front outwash fan deposits. In the Orrisdale Formation: O-1 basal diamict,
48 37   O-2 outwash deposits, O-3 subaqueous sands and muds, O-4 subaerial flow diamict. Subdivisions
49 38   for the Jurby Formation are not shown. Vertical scale much exaggerated and minor detail removed
50 39   for clarity. Ice margin still-stands in the Orrisdale Formation are marked OR1 to OR4.
51 40   Transgressive off-lapping ice margin readvance positions in the Jurby Formation are marked JH1
52 41   to JH4.
53
54

55 42   Fig 7. Detailed stratigraphy and lithofacies assemblages identifying the OSL samples from: A.
56 43   Orrisdale photographed 7/11/2013 (T3ORIS01), B. Dog Mills (T3DOGM01) and C. Jurby
57

58   29
59
60

1 (T3JURB01, T3JURB02). Site stratigraphies (after Thomas et al., 2004; Thomas et al., 2006) using

2 identical formation colours as Fig. 6. Lithofacies code annotations are as follows: S - sand, ASM -

3 alternating sand and mud, LM - laminated mud, MM - massive mud.

4 Fig. 8. A. Geomorphology and sampling around Gutterby-Annaside Banks and Black Combe. B.

5 Stratigraphical logs from the Gutterby sections T3GUTT01 and T3GUTT03.

6 Fig. 9. The Holme St Cuthbert ice contact delta on the Scottish Readvance limit. A. NW-SE Quarry

7 face at Aldoth Quarry in December 2013. B. Aldoth Quarry in the Holme St Cuthbert ice contact

8 delta complex. OSL samples, C. T3ALDO02 and D. T3ALDO01 respectively.

9 Fig. 10. Sea floor acoustic and stratigraphical data from east and north of the Isle of Man. A. the

10 location, zones and boundary limits, the JC106 cruise track (green), cores and transect lines x^1-x^2,

11 y^1-y^2 and y^2-y^3. B. East of the Isle of Man line x^1-x^2 the sub-bottom profiler data traverse the

12 glaciotectonic axis of the Bride Moraine. C. Line y^1-y^2 the sub-bottom profiler data extend from the

13 eastern Irish Sea mud basin to the Solway Firth. D. Planform multi-beam data with 2m contour

14 intervals, sub-bottom profiler data and the vibrocore stratigraphy from line y^2-y^3 in the Solway Firth.

15 The sub-bottom profiler data are annotated with acoustic facies (Table 6), boundaries and core

16 locations.

17 Fig. 11. Lithofacies examples from key acoustic facies sampled from vibrocore JC106-084VC from

18 line y2-y3 (Fig. 10D).

19 Fig. 12. Bayesian models for the dating of ice retreat across A. northeast Ireland and B. the

20 northeast Irish Sea Basin. The model structure shown uses OxCal brackets (left) and keywords

21 that define the relative order of events (Bronk Ramsey, 2009a). Each original distribution (hollow)

22 represents the relative probability of each age estimate with posterior density estimate (solid)

23 generated by the modelling. Shown are 14C ages (green), OSL ages (orange), CN ages (blue) and

24 modelled boundary ages (Red). Outliers are denoted by '?' and their probably (P) of being an

25 outlier indicated by low values <5 (95% confidence). Model agreement indices for individual ages

26 show their fit to the model with >60% the widely used threshold for 'good' fit (Bronk Ramsey,

27 2009a).

28 Fig. 13. A: The boundary ages (square ± 1 sigma whisker plots) from the Bayesian model against

29 net axial retreat distance plotted with summer insolation (red dots) for 60°N (Berger and Loutre,

30 1991). Arrows denote more substantial readvances of the ice margin associated with BL5 (Jurby-

31 Gutterby readvance) and BL6 (Scottish Readvance) in the overall dated retreat sequence. B: Likely

32 calving margin widths (pecked) and average trough elevation (solid) estimated as mean of 10 %

33 deepest depths from the EMODnet bathymetry (http://www.emodnet-hydrography.eu/) plotted

34 against the boundary ages. C: d18O concentrations and Greenland Interstadials (GI) from the

35 Greenland ice cores (Rasmussen et al., 2014) and modelled surface air temperatures relative to

36 the present for land masses north of ~45°N (Bintanja et al., 2005). D: SST records determined for

37 the North Atlantic using alkenones at 37°N 10°W (Bard, 2002) plotted using an updated age model

38 (Bard et al., 2004) and from Ocean Drilling Project (ODP) site 982 at 57°N 17°W (Lawrence et al.,

39 2009). Modelled RSL for Anglesey (blue dots) derived from the glacial isostatic adjustment (GIA)

40 model of Bradley et al. (2011). E: The dolomitic carbon (DC – solid orange) and total ice rafted

41 debris (IRD- grey outline) flux records from the OMEX2K marine core (Haapaniemi et al., 2010).

42 Heinrich Event H1 is highlighted (Bond et al., 1992).

43

Table 1. Environmental dose-rates were determined using ICP-MS and ICP-AES analysis and in situ gamma spectrometry. The chemical concentrations are presented in the decimal points to a precision relevant for the detection limit. The grain size for all samples was a 212 – 250 μm diameter, except for sample T3DOGM01 which was 150 – 180 μm. The dose-rates were calculated using the conversion factors of Guérin et al. (2011) and beta dose-rate attenuation factors of Guérin et al. (2012). Water contents were estimated considering the field and saturated water contents, and the environmental history for each sample; these values are expressed as a percentage of the mass of dry sediment. Cosmic dose-rates were determined after (Prescott and Hutton, 1994). Dose-rates were calculated using the Dose Rate and Age Calculator (DRAC: Durcan et al., 2015).

Sample	Depth (m)	Water content (%)	K (%)	Rb (ppm)	U (ppm)	Th (ppm)	Beta dose-rate (Gy/ka)	Gamma dose-rate (Gy/ka)	Cosmic dose-rate (Gy/ka)	Total dose-rate (Gy/ka)
T3TURK01	1.0	20 ± 5	1.1 ± 0.1	59.2 ± 5.9	1.44 ± 0.14	6.0 ± 0.6	0.87 ± 0.08	0.59 ± 0.04	0.18 ± 0.02	1.67 ± 0.09
T3BALH01	13.0	23 ± 5	0.9 ± 0.1	31.9 ± 3.2	0.76 ± 0.08	2.5 ± 0.3	0.62 ± 0.07	0.38 ± 0.02	0.05 ± 0.01	1.06 ± 0.07
T3BALH02	3.0	17 ± 5	0.8 ± 0.1	28.0 ± 2.8	0.59 ± 0.06	2.1 ± 0.2	0.57 ± 0.06	0.40 ± 0.03	0.14 ± 0.01	1.12 ± 0.07
T3ORIS01	5.0	17 ± 5	1.2 ± 0.1	30.1 ± 3.0	0.81 ± 0.08	2.5 ± 0.3	0.84 ± 0.09	0.44 ± 0.03	0.11 ± 0.01	1.40 ± 0.09
T3DOGM01	5.0	23 ± 5	1.5 ± 0.2	49.7 ± 5.0	1.53 ± 0.15	4.7 ± 0.5	1.10 ± 0.13	0.73 ± 0.05	0.11 ± 0.01	1.97 ± 0.14
T3JURB01	9.5	23 ± 5	1.0 ± 0.1	36.7 ± 3.7	0.85 ± 0.09	3.2 ± 0.3	0.69 ± 0.07	0.35 ± 0.02	0.07 ± 0.01	1.13 ± 0.07
T3JURB02	6.5	23 ± 5	1.1 ± 0.1	36.8 ± 3.7	0.72 ± 0.07	2.4 ± 0.2	0.73 ± 0.07	0.39 ± 0.03	0.09 ± 0.01	1.22 ± 0.08
T3GUTT01	20.0	30 ± 5	1.5 ± 0.2	61.5 ± 6.2	0.89 ± 0.09	3.0 ± 0.3	0.92 ± 0.09	0.49 ± 0.03	0.03 ± 0.00	1.44 ± 0.10
T3GUTT03	3.5	23 ± 5	1.5 ± 0.2	66.1 ± 6.6	0.96 ± 0.10	3.3 ± 0.3	0.99 ± 0.10	0.83 ± 0.05	0.13 ± 0.01	1.97 ± 0.11
T3ALDO01	1.0	20 ± 5	1.7 ± 0.2	53.5 ± 5.4	0.94 ± 0.09	3.5 ± 0.4	1.14 ± 0.13	0.71 ± 0.05	0.18 ± 0.02	2.04 ± 0.14
T3ALDO02	1.5	20 ± 5	1.1 ± 0.1	39.5 ± 4.0	0.88 ± 0.09	3.6 ± 0.4	0.78 ± 0.07	0.65 ± 0.04	0.17 ± 0.02	1.61 ± 0.09

1

1
2
3
4 1 Table 2. OSL analytical results. The overdispersion calculated from a dose-recovery (DR OD) experiment is given, and has been used to inform the
5 2 selection of the value of σ_b used for calculation of the minimum age model (MAM). The total number of grains analysed for dating are given, along
6 3 with the number of grains (n) yielding D_e values. The overdispersion (OD) of the D_e dataset measured for each sample is given along with the age
7 4 model used to generate the final D_e and age.
8
9

Sample	Grain size (µm)	DR OD (%)	Total analysed	n	OD (%)	Age model	σ_b	D_e (Gy)	Age (ka)
T3TURK01	212 – 250	17	1,600	50	56 ± 1	CAM	-	32.0 ± 2.8	19.2 ± 2.0
T3BALH01	212 – 250	14	1,900	49	72 ± 1	MAM	0.25	19.6 ± 3.2	18.5 ± 3.3
T3BALH02	212 – 250	-	2,000	65	55 ± 1	MAM	0.25	30.5 ± 3.9	27.1 ± 3.8
T3ORIS01	212 – 250	10	3,800	94	48 ± 1	MAM	0.20	33.3 ± 3.7	23.8 ± 3.1
T3DOGM01	150 – 180	0	1,800	80	53 ± 1	CAM	-	44.2 ± 2.9	22.5 ± 2.2
T3JURB01	212 – 250	8	4,000	105	52 ± 1	MAM	0.20	23.5 ± 2.3	20.8 ± 2.4
T3JURB02	212 – 250	-	2,800	83	46 ± 1	MAM	0.20	28.6 ± 2.9	23.4 ± 2.8
T3GUTT01	212 – 250	0	7,300	105	54 ± 1	MAM	0.20	38.9 ± 4.0	27.0 ± 3.3
T3GUTT03	212 – 250	-	5,600	77	45 ± 1	MAM	0.20	42.6 ± 4.5	21.7 ± 2.6
T3ALDO01	212 – 250	15	2,400	56	59 ± 1	MAM	0.25	41.2 ± 6.6	20.2 ± 3.5
T3ALDO02	212 – 250	-	2,800	64	59 ± 1	MAM	0.25	45.0 ± 7.1	27.9 ± 4.7

24 5
25
26 6
27
28
29
30
31
32
33
34
35
36
37
38
39
40
41 2
42
43
44
45

46
47

1
2
3
4 1 Table 3. Sample information and exposure ages for the new cosmogenic nuclide samples. calculated using an online calculator (version 2.3
5 2 https://hess.ess.washington.edu/) (Balco et al., 2008) with time-dependent Lm scaling (Lal, 1991; Stone, 2000) an erosion rate of 1 mm ka-1, and a
6 3 local production rate, the Loch Lomond production rate (LLPR) of 4.00 ± 0.17 atoms g-1 a-1 (Fabel et al., 2012).
7

Sample	Lat.	Long.	Alt. (m)	Thickness (cm)	Shielding[a]	^{10}Be conc. (at g^{-1})[b]	^{10}Be conc. ±	Exposure Age (ka)[c]	Exposure age (ka) –global[d]
T3CREG01	54.07156	-4.77349	155	2.5	0.998	97761	2981	**21.3 ± 1.2 (0.7)**	*20.8 ± 1.1 (0.6)*
T3CREG02	54.07156	-4.77349	155	3.8	1.000	95554	2523	**20.9 ± 1.1 (0.6)**	*20.6 ± 1.1 (0.6)*
T3BARR01	54.1509	-4.6677	475	0.9	0.989	156338	4554	**25.0 ± 1.3 (0.8)**	*24.5 ± 1.3 (0.7)*
T3BARR02	54.1507	-4.6548	385	2.4	0.995	108925	3040	**18.9 ± 1.0 (0.6)**	*18.6 ± 1.0 (0.5)*
T3BC02	54.25763	-3.35291	260	3.0	0.944	85360	2978	**17.7 ± 1.0 (0.6)**	*17.7 ± 1.0 (0.6)*
T3BC03	54.25768	-3.35315	255	3.0	0.982	121332	3582	**24.4 ± 1.3 (0.7)**	*24.4 ± 1.3 (0.7)*
T3BC05	54.25798	-3.35308	255	3.5	0.966	105849	3260	**21.7 ± 1.2 (0.7)**	*21.7 ± 1.2 (0.7)*
T3BC06	54.25698	-3.35303	255	2.5	0.978	111242	3766	**22.4 ± 1.3 (0.8)**	*22.4 ± 1.3 (0.8)*

4 [a] Calculated an online calculator (http://hess.ess.washington.edu/) (Balco et al., 2008).
5 [b] Be analyses were standardised to NIST27900 with ^{10}Be/^{9}Be taken as 2.79 x 10^{-11}. A process blank correction of 1.6 – 3.6% (53046 – 58050 atoms) was applied to
6 all samples.
7 [c] Exposure ages calculated using an online calculator (version 2.3 https://hess.ess.washington.edu/) (Balco et al., 2008) and Lm scaling, assuming a density
8 of 2.6 g cm^{-3}. Analytical uncertainties reported in parentheses. Ages calculated using the Loch Lomond production rate (Fabel et al., 2012).
9 [d] Exposure ages calculated using default global production rates in the same online calculator.
10

3

1
2
3
4 1   Table 4. Surface exposure ages re-calculated using an online calculator (version 2.3 https://hess.ess.washington.edu/) (Balco et al., 2008) with with
5 2   time-dependent Lm scaling (Lal, 1991; Stone, 2000)an erosion rate of 1 mm ka-1, and a local production rate, the Loch Lomond production rate
6 3   (LLPR) of 4.00 ± 0.17 atoms g-1 a-1 (Fabel et al., 2012). The highlighted samples (*) were identified as outliers in the original studies. Note that in the
7 4   original studies, Lm scaling factors were used by Ballantyne et al. (2013) while Du scaling factors were used by (McCarroll et al., 2010).
8
9

Sample	Isotope	Published ages (ka)	Analytical uncert (ka)	Uncert. (ka)	LLPR ages (ka)	Uncert. (ka)	Original publication
GB-02	^{10}Be	12.0*	1.1	1.2	12.0	1.2	Ballantyne et al. (2013)
GB-03	^{10}Be	14.7	1.0	1.2	14.8	1.2	Ballantyne et al. (2013)
GB-04	^{10}Be	15.0	0.6	0.9	15.1	0.9	Ballantyne et al. (2013)
GB-06	^{10}Be	14.7	1.2	1.4	14.7	1.4	Ballantyne et al. (2013)
GT-01	^{10}Be	14.1	0.6	1.8	15.1	0.9	McCarroll et al. (2010)
GT-2.1	^{10}Be	14.3	0.3	1.7	15.5	0.8	McCarroll et al. (2010)
GT-2.2	^{10}Be	14.3	0.5	1.8	15.3	0.8	McCarroll et al. (2010)
GT-03	^{10}Be	13.0*	0.4	1.6	14.0	0.7	McCarroll et al. (2010)

5

6

4

1
2
3
4   1   Table 5. Acoustic facies associations (AFA) and the supporting lithostratigraphy from vibrocores for seismic lines in the northern ISB (Fig. 10A). These AFAs are
5   2   used as annotation on seismic lines on Fig. 10, and examples of the deposits associated with AFA 1a, 1c and 2 from vibrocore JC106-084VC are shown on Fig. 11.
6

Acoustic Facies	Lithostratigraphy	Environment and processes
AFA 1a	Overconsolidated sandy matrix supported pebbly diamicton (Dmm)	Irish Sea Till, subglacial diamict
AFA 1b	Overconsolidated sands (Sh) and gravels (Gm, Gms), including planar and trough cross-stratified units (Gp, Sp, Gt, St)	Glaciofluvial outwash, occasionally tectonised and overconsolidated
AFA 1c	Overconsolidated occasionally laminated muds with dropstones (Dml)	Ice proximal outwash, affected by iceberg calving, overridden by ice
AFA 1d	Sands and silts (Sh and Fl), normally-consolidated, often bedded (1-10mm) occasionally massive (Sm)	Ice proximal outwash, either subaerial or efflux jet discharge from the ice margin, occasionally tectonised and overconsolidated
AFA 2	Normally-consolidated, laminated muds, silts and clays (Fl)	Ice distal suspension rain-out in a subaqueous basin
AFA 3	Glacitectonised (AFA 3), laminated muds, silts and clays (Fl)	Ice distal suspension deformed and glacitectonised by advancing ice
AFA 4	Unconsolidated shelly sands and gravels	Holocene shell-hash, sands and gravels worked by marine currents

3

4

5

1

Table 6. The original, modelled and boundary limit ages for each stage, all as ±1 sigma. * denotes ages identified as outliers that did not influence the modelled

2

outputs. On the left boundary ages with Zone 5/6 grouped as single Phase and on the right boundary ages with Zones 5 and 6 defined as separate Phases.

Prior	Age (ka)	*Modelled age (ka)*	Prior	Age (ka)	*Modelled age (ka)*	Interpretation
Boundary Limit 1		*21.4 ± 1.0*	Boundary Limit 1		*21.4 ± 1.0*	Retreat northwards from NW Wales
Zone 1 North Wales			Zone 1 North Wales			Ice margins moving northwards from the north Wales coast towards the Isle of Man
T4ABER01	18.1 ± 1.6	*21.0 ± 0.8*	T4ABER01	18.1 ± 1.6	*21.1 ± 0.7*	
T4ABER03	20.2 ± 1.9	*21.0 ± 0.8*	T4ABER03	20.2 ± 1.9	*21.1 ± 0.7*	
Boundary Limit 2		*20.7 ± 0.7*	Boundary Limit 2		*20.8 ± 0.7*	Retreat to the southern Isle of Man
Zone 2 South Isle of Man			Zone 2 South Isle of Man			
T3BARR01*	25.0 ± 1.3	*	T3BARR01*	25.0 ± 1.3	*	High altitude boulders on the summits of the Isle of Man
T3BARR02*	18.9 ± 1.0	*	T3BARR02*	18.9 ± 1.0	*	
T3CREG01	21.3 ± 1.2	*20.5 ± 0.7*	T3CREG01	21.3 ± 1.2	*20.6 ± 0.6*	
T3CREG02	20.9 ± 1.1	*20.5 ± 0.7*	T3CREG02	20.9 ± 1.1	*20.6 ± 0.6*	Landfall of ice margins on the southern lowlands of the Isle of Man
T3TURK01	19.2 ± 2.0	*20.4 ± 0.7*	T3TURK01	19.2 ± 2.0	*20.6 ± 0.7*	
T3BC02*	17.7 ± 1.0	*	T3BC02*	17.7 ± 1.0	*	
T3BC03*	24.4 ± 1.3	*	T3BC03*	24.4 ± 1.3	*	High altitude boulders in coastal western Cumbria
T3BC05*	21.7 ± 1.2	*	T3BC05*	21.7 ± 1.2	*	
T3BC06*	22.4 ± 1.3	*	T3BC06*	22.4 ± 1.3	*	
Boundary Limit 3		*20.2 ± 0.7*	Boundary Limit 3		*20.3 ± 0.7*	Retreat to the Central Valley, Isle of Man
Zone 3 Central Isle of Man			Zone 3 Central Isle of Man			Ice impinging on the Peel embayment, central Isle of Man
T3BALH01	18.5 ± 3.3	*19.9 ±0.7*	T3BALH01	18.5 ± 3.3	*20.1 ± 0.7*	
T3BALH02*	27.1 ± 3.8	*	T3BALH02*	27.1 ± 3.8	*	
Boundary Limit 4		*19.6 ± 0.8*	Boundary Limit 4		*19.9 ± 0.7*	Retreat to Orrisdale
Zone 4 Orrisdale			Zone 4 Orrisdale			Ice margins within the Orrisdale Formation, a series of still-stands in the retreat sequence
T3ORIS01	23.8 ± 3.1	*19.3 ±0.9*	T3ORIS01	23.8 ± 3.1	*19.6 ± 0.8*	
T3DOGM01	22.5 ± 2.2	*22.7 ± 2.1*	T3DOGM01	22.5 ± 2.2	*22.8 ± 2*	
Boundary Limit 5		*18.9 ± 1.0*	Boundary Limit 5		*19.3 ± 0.8*	Predating the Jurby – Gutterby readvance
Zone 5/6 Scottish Readvance			Zone 5 Jurby – Gutterby			A substantial readvance episode, on the Isle of Man laying down an on-lapping contiguous transgressive sequence of four limit positions
			T3JURB01	20.8 ± 2.4	*18.8 ± 0.9*	
T3JURB01	20.8 ± 2.4	*17.8 ± 1.1*	T3JURB02	23.4 ± 2.8	*18.9 ± 0.9*	
T3JURB02	23.4 ± 2.8	*17.9 ± 1.1*	T3GUTT03	21.7 ± 2.6	*18.9 ± 0.9*	
T3GUTT03	21.7 ± 2.6	*17.9 ± 1.1*	Boundary Limit 6		*18.3 ± 1.1*	Predating the Scottish readvance
T3ALDO01	20.2 ± 3.5	*17.6 ± 1.2*	Zone 6 Scottish Readvance			Readvance of Scottish ice an unknown distance from the Solway Firth into lowland Cumbria
T3ALDO02*	27.9 ± 4.7	*	T3ALDO01	20.2 ± 3.5	*17.1 ± 1.1*	
			T3ALDO02*	27.9 ± 4.7	*	
Boundary Limit 7		*15.9 ± 0.7*	Boundary Limit 7		*15.5 ± 0.6*	Retreat to the Galloway Hills
Zone 7 Galloway Hills			Zone 7 Galloway Hills			
GB-02*	12.0 ± 1.2	*	GB-02*	12.0 ± 1.2	*	
GB-03	14.8 ± 1.2	*15.1 ± 0.6*	GB-03	14.8 ± 1.2	*15.0 ± 0.5*	
GB-04	15.1 ± 0.9	*15.2 ± 0.5*	GB-04	15.1 ± 0.9	*15.1 ± 0.5*	Deglaciation of an ice dome over the Galloway Hills ice and a key interior source for Irish Sea ice
GB-06	14.7 ± 1.4	*15.1 ± 0.6*	GB-06	14.7 ± 1.4	*15.0 ± 0.5*	
GT-01	15.1 ± 0.9	*15.2 ± 0.5*	GT-01	15.1 ± 0.9	*15.1 ± 0.5*	
GT-2.1	15.5 ± 0.8	*15.2 ± 0.5*	GT-2.1	15.5 ± 0.8	*15.1 ± 0.5*	
GT-2.2	15.3 ± 0.8	*15.2 ± 0.5*	GT-2.2	15.3 ± 0.8	*15.1 ± 0.5*	
GT-03	14.0 ± 0.7	*14.9 ± 0.5*	GT-03	14.0 ± 0.7	*14.9 ± 0.5*	
Boundary Limit 8		*14.5 ± 0.6*	Boundary Limit 8		*14.6 ± 0.6*	Deglaciated Galloway Hills ice dome

3

6

Fig. 1. Location and context of the northern Irish Sea Basin plotted on Nextmap™ and EMODnet topographical data (http://www.emodnet-hydrography.eu/). This shows inferred ice margins (red and white) including the possible extent of the calving margins. Triangles denote cores and geophysical survey lines (black dashed lines) taken on the cruise JC106 and the locations of dating sites. The zones (1-7) and boundaries (BL1 to 7) used the chronological model are identified.

124x86mm (300 x 300 DPI)

Fig. 2. Abanico plots of the De values determined for OSL dating. Note that sample T3DOGM01 was analysed using microhole analyses (i.e. up to four grains in each hole due to a grain size of 150 – 180 µm) rather than single grains and so the CAM provides a maximum OSL age for this sample. The abanico plots shown present the De distributions in two plots that share a common z-axis of De values: (1) a bivariate plot where each De value is presented in relation to its precision (shown on the x-axis, where those more precisely known have greater values of precision); this is similar to the radial plot commonly used in luminescence dating; and (2) a univariate plot showing the age frequency distribution of De values, which does not give any presentation of the precision of individual De values. The grey shading across both plots shows the CAM or MAM De for each distribution (± 2 σ shown on the y-axis). The combination of these two plots aids interpretation of the scatter in the De distributions, where samples with a greater range of De values on the z-axis have larger amounts of scatter in the De distribution.

256x340mm (300 x 300 DPI)

1
2
3
4
5
6
7
8
9
10
11
12
13
14
15
16
17
18
19
20
21
22
23
24
25
26
27
28
29
30
31
32
33
34
35
36
37
38
39
40
41
42
43
44
45
46
47
48
49
50
51
52
53
54
55
56
57
58
59
60

Fig. 3. Glacial geomorphology of the south of the Isle of Man and a 5 km Ordnance Survey grid (Roberts et al., 2007; Thomas et al., 2006) showing the locations of samples T3CREG01 and T3CREG02, T3TURK01 and T3BARR01 and T3BARR02.

135x106mm (300 x 300 DPI)

Fig. 4. Cosmogenic nuclide samples: A. T3BARR01 from the summit of South Barrule, B. T3BARR02 from the flanks of South Barrule on the Isle of Man. C-F. Samples from Black Combe in coastal Cumbria, NW England.

453x544mm (96 x 96 DPI)

Fig. 5. A. Glacial geomorphology of the Peel Embayment, central Isle of Man (after Thomas et al., 2006) and a 1 km Ordnance Survey grid, showing the locations of samples T3BALH01 and T3BALH02. B. Quarry section photographs, summary stratigraphy and lithofacies at Ballaharra quarry on 7/11/2013, and samples C. T3BALH01 and D. T3BALH02.

85x42mm (300 x 300 DPI)

Fig. 6. Lithostratigraphy of the Northern Plain of the Isle of Man (after Thomas et al., 2004; Thomas et al., 2006) with a 5 km Ordnance Survey grid. Summary stratigraphy and lithofacies assemblages on the east and west coasts of the Northern Plain of the Isle of Man, identifying the OSL sample locations from Orrisdale (T3ORIS01), Dog Mills (T3DOGM01) and Jurby (T3JURB01, T3JURB02). Stratigraphical sections show the three major glacigenic formations (from oldest to youngest: the Shellag, Orrisdale and Jurby Formations). Stratigraphic units comprise in the Shellag Formation: S1 basal diamict; S2 ice front outwash fan deposits. In the Orrisdale Formation: O-1 basal diamict, O-2 outwash deposits, O-3 subaqueous sands and muds, O-4 subaerial flow diamict. Subdivisions for the Jurby Formation are not shown. Vertical scale much exaggerated and minor detail removed for clarity. Ice margin still-stands in the Orrisdale Formation are marked OR1 to OR4. Transgressive off-lapping ice margin readvance positions in the Jurby Formation are marked JH1 to JH4.

242x292mm (300 x 300 DPI)

1
2
3
4
5
6
7
8
9
10
11
12
13
14
15
16
17
18
19
20
21
22
23
24
25
26
27
28
29
30
31
32
33
34
35
36
37
38
39
40
41
42
43
44
45
46
47
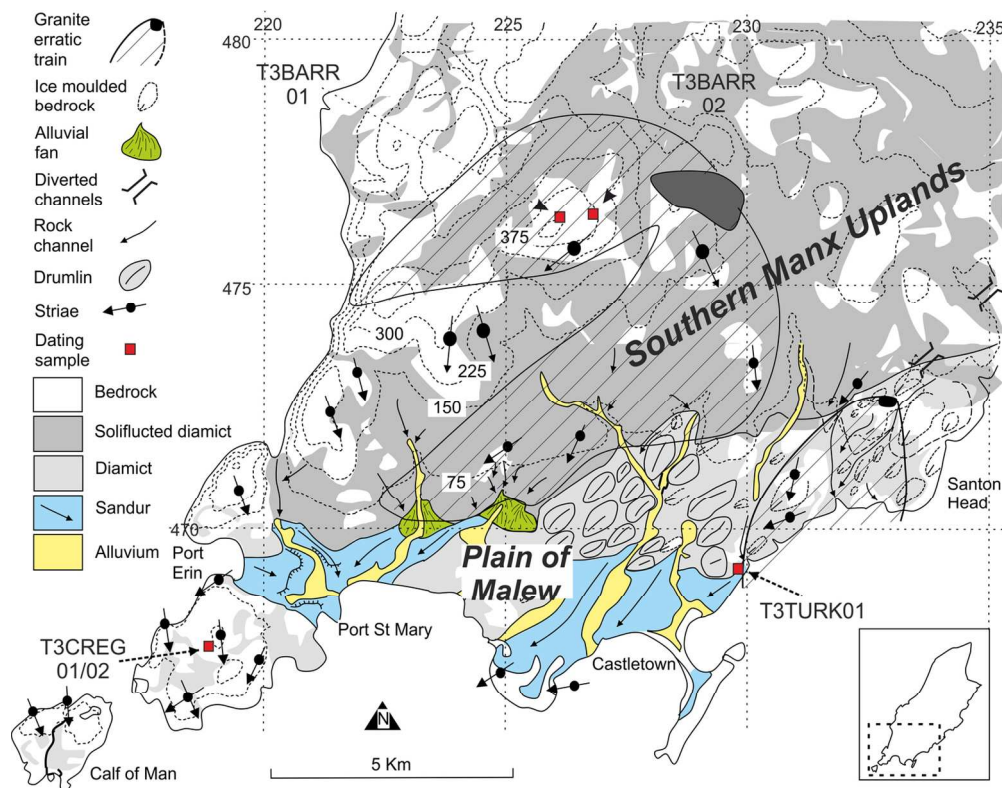48
49
50
51
52
53
54
55
56
57
58
59
60

Fig 7. Detailed stratigraphy and lithofacies assemblages identifying the OSL samples from: A. Orrisdale photographed 7/11/2013 (T3ORIS01), B. Dog Mills (T3DOGM01) and C. Jurby (T3JURB01, T3JURB02). Site stratigraphies (after Thomas et al., 2004; Thomas et al., 2006) using identical formation colours as Fig. 6. Lithofacies code annotations are as follows: S - sand, ASM - alternating sand and mud, LM - laminated mud, MM - massive mud.

150x140mm (300 x 300 DPI)

Fig. 8. A. Geomorphology and sampling around Gutterby-Annaside Banks and Black Combe. B. Stratigraphical logs from the Gutterby sections T3GUTT01 and T3GUTT03.

99x57mm (300 x 300 DPI)

Fig. 9. The Holme St Cuthbert ice contact delta on the Scottish Readvance limit. A. NW-SE Quarry face at Aldoth Quarry in December 2013. B. Aldoth Quarry in the Holme St Cuthbert ice contact delta complex. OSL samples, C. T3ALDO02 and D. T3ALDO01 respectively.

111x71mm (300 x 300 DPI)

Fig. 10. Sea floor acoustic and stratigraphical data from east and north of the Isle of Man. A. the location, zones and boundary limits, the JC106 cruise track (green), cores and transect lines x1-x2, y1-y2 and y2-y3. B. East of the Isle of Man line x1-x2 the sub-bottom profiler data traverse the glaciotectonic axis of the Bride Moraine. C. Line y1-y2 the sub-bottom profiler data extend from the eastern Irish Sea mud basin to the Solway Firth. D. Planform multi-beam data with 2m contour intervals, sub-bottom profiler data and the vibrocore stratigraphy from line y2-y3 in the Solway Firth. The sub-bottom profiler data are annotated with acoustic facies (Table 6), boundaries and core locations.

220x278mm (300 x 300 DPI)

Fig. 11. Lithofacies examples from key acoustic facies sampled from vibrocore JC106-084VC from line y2-y3 (Fig. 10D).

126x162mm (300 x 300 DPI)

Fig. 12. Bayesian models for the dating of ice retreat across A. northeast Ireland and B. the northeast Irish Sea Basin. The model structure shown uses OxCal brackets (left) and keywords that define the relative order of events (Bronk Ramsey, 2009a). Each original distribution (hollow) represents the relative probability of each age estimate with posterior density estimate (solid) generated by the modelling. Shown are 14C ages (green), OSL ages (orange), CN ages (blue) and modelled boundary ages (Red). Outliers are denoted by '?' and their probably (P) of being an outlier indicated by low values <5 (95% confidence). Model agreement indices for individual ages show their fit to the model with >60% the widely used threshold for 'good' fit (Bronk Ramsey, 2009a).

111x71mm (300 x 300 DPI)

Fig. 13. A: The boundary ages (square ± 1 sigma whisker plots) from the Bayesian model against net axial retreat distance plotted with summer insolation (red dots) for 60°N (Berger and Loutre, 1991). Arrows denote more substantial readvances of the ice margin associated with BL5 (Jurby-Gutterby readvance) and BL6 (Scottish Readvance) in the overall dated retreat sequence. B: Likely calving margin widths (pecked) and average trough elevation (solid) estimated as mean of 10 % deepest depths from the EMODnet bathymetry (http://www.emodnet-hydrography.eu/) plotted against the boundary ages. C: d18O concentrations and Greenland Interstadials (GI) from the Greenland ice cores (Rasmussen et al., 2014) and modelled surface air temperatures relative to the present for land masses north of ~45°N (Bintanja et al., 2005). D: SST records determined for the North Atlantic using alkenones at 37°N 10°W (Bard, 2002) plotted using an updated age model (Bard et al., 2004) and from Ocean Drilling Project (ODP) site 982 at 57°N 17°W (Lawrence et al., 2009). Modelled RSL for Anglesey (blue dots) derived from the glacial isostatic adjustment (GIA) model of Bradley et al. (2011). E: The dolomitic carbon (DC – solid orange) and total ice rafted debris (IRD- grey outline) flux records from the OMEX2K marine core (Haapaniemi et al., 2010). Heinrich Event H1 is highlighted (Bond et al., 1992).

173x123mm (150 x 150 DPI)

SUPPLEMENTARY MATERIAL

ICE MARGIN OSCILLATIONS DURING DEGLACIATION OF THE NORTHERN IRISH SEA BASIN

R.C. Chiverrell[1*], R.K. Smedley[1,], D. Small[2], C.K. Ballantyne[3], M.J. Burke[1], S.L. Callard[2], C.D. Clark[4], G.A.T. Duller[5], D.J.A. Evans[2], D. Fabel[6], K. van Landeghem[7], S. Livingstone[4], Ó Cofaigh, C.[2], G.S.P. Thomas[1]. D.H. Roberts[2], M Saher[7], J.D. Scourse[8], P. Wilson[9]

[1]School of Environmental Sciences, University of Liverpool, Liverpool, UK

[2]Department of Geography, Durham University, Durham, UK

[3]School of Geography and Sustainable Development, University of St Andrews, St Andrews, UK

[4]Department of Geography, University of Sheffield, Sheffield, UK

[5]Department of Geography and Earth Sciences, Aberystwyth University, Ceredigion, UK

[6]Scottish Universities Environmental Research Centre, East Kilbride, UK

[7]School of Ocean Sciences, Bangor University, Menai Bridge, Anglesey, UK

[8]College of Life and Environmental Science, University of Exeter, Cornwall, UK

[9]School of Geography and Environmental Sciences, University of Ulster, Coleraine, UK

(*E-mail: RCHIV@LIV.AC.UK)

BAYESIAN MODELLING CODE

```
Options()
 {
  BCAD=FALSE;
 };
 Plot()
 {
  Outlier_Model("T3-ISB
East", T(5), U(0,4), t);
  Sequence("Retreat T3
Britice-chrono")
  {
   Boundary("Boundary Limit
1")
   {
    color="Red";
   };
   Phase("Zone 1
Aberogwen")
   {
    Phase("Aber Ogwen")
    {
     C_Date("T4ABER03",
20200, 1900)
     {
      color="Orange";
      Outlier("Test", 0.2);
     };
     C_Date("T4ABER01",
18100, 1600)
     {
      color="Orange";
      Outlier("Test", 1);
     };
    };
   };
   Boundary("Boundary Limit
2")
   {
    color="Red";
   };
   Phase("Zone 2 South Isle
of Man")
   {
    C_Date("T3BARR01",
25000, 1300)
    {
     color="Blue";
     Outlier();
    };
    C_Date("T3BARR02",
18900, 1000)
    {
     Outlier();
     color="Blue";
    };
    C_Date("T3CREG01",
21300, 1200)
    {
     Outlier("Test", 0.2);
     color="Blue";
    };
    C_Date("T3CREG02",
20900, 1100)
    {
     Outlier("Test", 0.2);
     color="Blue";
    };
    C_Date("T3TURK01",
19200, 2000)
    {
     Outlier("Test", 0.2);
     color="Orange";
    };
   };
   Phase("Zone 1-5
Lowering")
   {
    C_Date("T3BC02",
17700, 1000)
    {
     Outlier();
     color="Blue";
    };
    C_Date("T3BC03",
24400, 1300)
    {
     Outlier();
     color="Blue";
    };
    C_Date("T3BC05",
21700, 1200)
    {
```

```
  Outlier();
  color="Blue";
};
C_Date("T3BC06",
22400, 1300)
  {
  Outlier();
  color="Blue";
  };
};
Boundary("Boundary Limit
3")
{
  color="Red";
};
Phase("Zone 3 Central
Isle of Man")
{
  C_Date("T3BALH02",
27100, 3800)
  {
  color="Orange";
  Outlier();
  };
  C_Date("T3BALH01",
18500, 3300)
  {
  color="Orange";
  Outlier("Test", 0.2);
  };
};
Boundary("Boundary Limit
4")
{
  color="Red";
};
Phase("Zone 4 Orrisdale
oscillations")
{
  C_Date("T3ORIS01",
23800, 3100)
  {
  color="Orange";
  Outlier("Test", 0.2);
  };
  After("Dog Mills")
  {
  C_Date("T3DOGM01",
22500, 2200)
  {
  color="Orange";
  Outlier("Test", 0.2);
  };
  };
};

Boundary("Boundary Limit
5")
{
  color="Red";
};
Phase("Zone 5 Scottish
(?) readvance")
{
  C_Date("T3JURB01",
20800, 2400)
  {
  color="Orange";
  Outlier("Test", 0.2);
  };
  C_Date("T3JURB02",
23400, 2800)
  {
  color="Orange";
  Outlier("Test", 1);
  };
  C_Date("T3GUTT03",
21700, 2600)
  {
  color="Orange";
  Outlier("Test", 0.2);
  };
};
Boundary("Boundary Limit
6")
{
  color="Red";
};
Phase("Zone 5 Scottish
(?) readvance")
{
  C_Date("T3ALDO01",
20200, 3500)
  {
  color="Orange";
  Outlier("Test", 0.2);
  };
  C_Date("T3ALDO02",
27900, 4700)
  {
  Outlier();
  color="Orange";
  };
};
Boundary("Boundary Limit
7")
{
  color="Red";
};
Phase("Zone 6 Galloway
Hills")
{

C_Date("GB-02", 12000,
1200)
  {
  color="Blue";
  Outlier();
  };
C_Date("GB-03", 14800,
1200)
  {
  color="Blue";
  Outlier("Test", 0.2);
  };
C_Date("GB-04", 15100,
900)
  {
  color="Blue";
  Outlier("Test", 0.2);
  };
C_Date("GB-06", 14700,
1400)
  {
  Outlier("Test", 0.2);
  color="Blue";
  };
C_Date("GT-01", 15100,
900)
  {
  color="Blue";
  Outlier("Test", 0.2);
  };
C_Date("GT-2.1", 15500,
800)
  {
  color="Blue";
  Outlier("Test", 0.2);
  };
C_Date("GT-2.2", 15300,
800)
  {
  color="Blue";
  Outlier("Test", 0.2);
  };
C_Date("GT-03", 14000,
700)
  {
  color="Blue";
  Outlier("Test", 0.2);
  };
};
Boundary("Boundary Limit
8")
{
  color="Red";
};
};
};
```

D$_e$ VALUES DETERMINED FOR OSL DATING

Table S1. D$_e$ values from OSL dating of sample T3TURK01.

D$_e$ (Gy)	D$_e$ Uncertainty (Gy)	Net T$_n$ signal in response to 10.6 Gy (cts/0.1 s)
4.56	4.09	78
35.11	5.11	259
35.75	6.69	3954
124.68	15.54	359
38.01	9.95	72
7.81	3.41	61
18.20	4.26	107
13.37	3.58	67
48.08	7.13	351
28.55	2.94	371
25.24	2.18	1829
97.35	10.48	1598
36.18	3.22	805
16.78	2.42	292
72.18	17.55	100
7.55	3.61	97
32.41	20.12	70
28.11	3.48	1231
83.25	31.69	3754
46.40	9.92	75
11.72	5.98	80
32.50	3.82	282
78.59	19.87	125
23.20	3.57	288
31.44	2.10	1328
27.61	5.27	91
39.77	10.21	874
2.89	6.58	58
23.91	6.01	59
45.17	25.06	81
31.64	4.85	211
131.92	20.34	1574

34.03	4.92	509
17.33	3.22	389
33.97	3.87	249
49.42	11.96	124
24.70	7.01	63
22.68	3.44	230
34.77	2.54	678
32.15	7.08	66
61.48	6.36	563
40.42	6.75	240
13.83	3.38	189
3.82	2.53	119
12.29	3.39	104
50.34	9.94	110
36.71	4.32	256
38.14	6.35	195
37.76	14.31	77
25.89	2.12	657
8.98	22.50	81

Table S2. D_e values from OSL dating of sample T3BALH01.

D_e (Gy)	D_e Uncertainty (Gy)	Net T_n signal in response to 12.9 Gy (cts/0.1 s)
187.98	14.25	2998
100.13	18.92	77
73.03	14.64	129
24.51	6.00	69
8.82	2.63	122
12.88	5.88	65
9.79	3.72	54
67.12	12.93	113
67.31	11.84	106
148.27	48.01	157
67.74	20.04	62
57.27	11.83	72

1
2
3   31.12   7.47   320
4
5   99.20   28.96   613
6
7   29.58   4.93   124
8
9   33.67   9.47   138
10
11   95.38   30.85   197
12
13   113.02   6.93   1771
14
15   71.23   20.40   60
16
17   22.30   6.13   338
18
19   100.47   25.08   71
20
21   21.99   6.55   78
22
23   58.30   4.34   1096
24
25   112.52   25.35   1770
26
27   148.57   34.25   87
28
29   27.74   10.46   198
30
31   29.93   4.73   133
32
33   19.56   2.70   177
34
35   75.80   5.65   2267
36
37   54.34   5.33   1510
38
39   65.37   27.58   52
40
41   163.20   22.41   924
42
43   52.66   16.84   243
44
45   47.86   15.86   66
46
47   60.80   14.42   61
48
49   30.66   3.80   195
50
51   31.89   7.36   389
52
53   29.28   10.47   73
54
55   25.23   5.60   68
56
57
58
59
60

31.12   7.47   320

Col 1	Col 2	Col 3
31.12	7.47	320
99.20	28.96	613
29.58	4.93	124
33.67	9.47	138
95.38	30.85	197
113.02	6.93	1771
71.23	20.40	60
22.30	6.13	338
100.47	25.08	71
21.99	6.55	78
58.30	4.34	1096
112.52	25.35	1770
148.57	34.25	87
27.74	10.46	198
29.93	4.73	133
19.56	2.70	177
75.80	5.65	2267
54.34	5.33	1510
65.37	27.58	52
163.20	22.41	924
52.66	16.84	243
47.86	15.86	66
60.80	14.42	61
30.66	3.80	195
31.89	7.36	389
29.28	10.47	73
25.23	5.60	68
75.47	10.90	159
74.77	9.39	487
137.21	13.99	490
99.00	16.90	238
81.39	5.56	1869

15.23	1.94	273
76.30	11.88	127
16.59	2.09	837
183.92	18.78	448
32.63	5.10	107

Table S3. D_e values from OSL dating of sample T3BALH02.

D_e (Gy)	D_e Uncertainty (Gy)	Net T_n signal in response to 12.9 Gy (cts/0.1 s)
11.61	20.94	67
32.29	8.48	65
48.99	14.74	38
115.56	13.83	192
33.28	6.85	111
63.08	8.78	2503
25.53	2.54	568
53.73	14.12	58
110.53	32.85	100
115.40	8.30	1145
73.94	11.39	107
92.90	25.18	99
41.98	14.75	103
6.58	20.74	127
77.48	9.79	286
70.72	6.93	417
40.10	6.08	130
23.20	6.19	125
14.50	5.46	76
54.57	19.98	84
23.13	6.78	64
135.42	33.39	2714
101.10	14.29	185
116.50	113.46	79

42.00	10.01	59
43.89	8.79	95
105.29	21.15	205
26.03	3.64	162
39.70	3.78	377
48.47	9.56	244
154.56	163.20	46
35.13	5.96	81
170.23	18.91	287
135.15	42.70	49
17.75	21.83	107
89.83	12.35	1015
88.15	49.48	41
60.97	9.47	375
58.05	19.08	83
83.99	23.93	99
158.29	27.15	76
20.70	4.50	107
56.95	17.43	49
63.55	11.80	238
33.96	5.26	218
82.77	4.60	1356
41.42	23.06	115
33.88	8.55	94
23.71	1.39	7739
63.76	8.69	212
173.07	23.50	120
78.59	10.69	3131
67.09	17.31	90
148.42	13.86	874
33.64	6.66	98
80.62	17.22	46

40.50	10.02	75
84.32	8.42	321
21.63	3.71	110
37.63	9.76	55
122.40	22.67	531
43.97	9.90	141
81.57	6.21	781
132.02	83.84	39
64.31	10.99	132

Table S4. D_e values from OSL dating of sample T3ORIS01.

D_e (Gy)	D_e Uncertainty (Gy)	Net T_n signal in response to 10.6 Gy (cts/0.1 s)
141.05	21.45	148
80.24	40.18	130
0.66	1.50	159
0.01	1.51	190
10.96	5.60	63
53.62	8.45	1069
48.81	10.32	77
69.59	12.99	116
58.33	30.66	52
17.94	6.34	69
9.31	4.95	68
30.01	4.37	817
91.35	37.53	943
62.18	17.12	75
36.92	3.78	278
38.28	7.76	380
56.83	8.10	169

70.78	21.35	75
32.73	11.99	76
40.56	8.86	122
142.61	35.26	669
83.75	24.85	658
52.90	17.03	270
29.60	7.29	414
38.82	2.84	3463
36.56	7.11	258
68.63	17.85	199
75.38	21.53	105
81.66	8.34	1770
62.25	8.26	288
41.47	8.03	144
31.59	4.02	201
61.01	15.50	889
62.21	18.41	73
98.07	7.73	462
15.14	4.09	74
33.29	6.94	121
131.02	14.33	347
42.41	2.44	1414
55.79	6.28	418
40.45	5.38	320
57.53	11.79	102
38.35	6.57	258
135.88	27.96	235

1
2
3
4
5
6
7
8
9
10
11
12
13
14
15
16
17
18
19
20
21
22
23
24
25
26
27
28
29
30
31
32
33
34
35
36
37
38
39
40
41
42
43
44
45
46
47
48
49
50
51
52
53
54
55
56
57
58
59
60

70.99	14.29	120
85.04	18.52	78
67.33	9.25	284
38.21	2.71	649
69.03	14.55	1157
42.11	6.16	190
33.37	9.54	65
44.38	2.73	3225
130.60	33.82	205
50.70	46.35	205
100.64	15.33	204
72.45	12.20	85
24.27	12.02	50
68.14	9.45	529
82.20	44.28	66
44.09	8.12	86
90.79	31.49	62
34.60	5.95	192
96.67	22.56	112
78.31	18.13	110
55.42	13.50	98
26.55	19.70	56
21.65	4.00	81
92.75	23.16	84
26.56	9.62	60
56.50	5.72	384
94.06	13.33	544

37.60	8.35	321
24.85	9.85	51
97.60	18.81	156
132.22	13.32	268
139.89	19.17	111
102.09	22.59	81
24.84	6.87	51
103.17	27.73	56
58.97	9.13	137
129.26	15.95	313
45.80	5.88	142
37.23	11.13	103
37.80	7.15	200
108.27	81.65	188
70.89	15.31	247
30.25	4.47	184
30.16	23.28	49
54.38	31.15	74
45.32	4.20	819
45.38	7.84	103
89.42	12.04	178
74.02	6.00	554
9.42	5.52	31

Table S5. D_e values from OSL dating of sample T3DOGM01.

D_e (Gy)	D_e Uncertainty (Gy)	Net T_n signal in response to 12.9 Gy (cts/0.1 s)
51.32	3.63	1393

37.25	8.79	62
23.71	3.01	261
34.32	10.55	40
84.35	18.35	66
45.06	7.98	161
43.87	35.20	123
99.13	18.01	2331
128.35	33.40	286
52.75	7.15	142
37.66	15.16	86
21.54	2.32	462
78.62	16.89	114
51.61	11.64	68
52.65	9.00	242
67.03	9.28	110
61.27	6.28	791
55.10	18.89	37
30.28	3.99	162
62.35	8.01	295
50.41	79.18	53
16.46	6.66	53
20.65	3.40	103
43.63	17.59	79
58.12	6.01	2112
35.95	8.21	395
35.48	4.36	208
41.79	2.11	6054

48.62	13.67	65
62.54	14.84	97
53.15	12.81	50
35.13	7.72	86
42.54	20.38	40
112.57	22.98	56
95.21	68.82	139
87.37	24.27	37
33.93	3.77	266
10.63	7.83	129
62.96	15.22	61
40.88	3.34	612
127.29	8.74	755
42.37	8.05	106
18.39	11.87	56
27.31	3.06	318
26.65	19.75	54
35.28	5.61	117
77.92	7.76	284
52.79	12.43	71
151.78	37.00	56
30.30	1.94	5672
30.23	24.19	128
34.50	4.13	239
41.75	16.46	82
23.34	12.93	55
34.28	9.02	64

29.84	8.25	47
32.38	4.12	305
72.09	53.80	82
56.23	9.04	329
106.45	19.01	483
39.87	7.21	171
28.21	16.77	44
122.79	23.18	111
27.65	6.75	54
32.82	10.32	186
28.74	3.92	156
59.32	18.96	49
21.32	5.44	66
31.40	5.46	196
47.90	10.70	53
63.24	13.72	211
64.08	17.29	89
64.22	17.83	210
54.34	9.78	120
96.12	77.00	73
82.65	18.89	88
43.92	14.25	95

Table S6. D_e values from OSL dating of sample T3JURB01.

D_e (Gy)	D_e Uncertainty (Gy)	Net T_n signal in response to 10.6 Gy (cts/0.1 s)
73.05	8.76	127
23.67	5.90	80
31.11	9.10	61

1
2
3
4
5
6
7
8
9
10
11
12
13
14
15
16
17
18
19
20
21
22
23
24
25
26
27
28
29
30
31
32
33
34
35
36
37
38
39
40
41
42
43
44
45
46
47
48
49
50
51
52
53
54
55
56
57
58
59
60

54.10	11.85	87
45.41	19.28	126
25.99	1.63	1604
91.43	19.89	134
45.16	18.28	77
45.08	7.85	163
79.42	16.72	92
33.57	5.51	189
48.49	10.23	124
26.16	13.76	104
57.95	18.35	92
86.91	12.25	22564
101.59	8.28	585
30.53	11.21	50
59.59	31.28	92
43.49	15.12	67
134.50	28.21	103
86.79	9.59	893
34.63	5.21	429
58.10	12.86	103
101.69	20.54	137
151.35	27.46	86
42.99	13.41	108
57.68	7.06	446
60.80	7.14	375
45.20	10.76	506
85.60	20.39	119

32.58	6.16	213
98.84	8.68	1841
73.13	8.07	362
16.77	2.25	262
62.12	9.45	245
37.33	4.30	313
102.06	31.27	68
34.90	4.58	559
70.18	22.93	121
118.70	19.16	101
133.84	14.28	604
21.26	1.26	1621
25.76	4.14	530
70.67	6.92	6430
34.88	6.12	106
82.31	13.96	279
39.13	7.48	309
51.17	55.59	97
23.77	5.90	71
97.20	33.76	135
88.08	49.17	62
75.79	9.71	259
39.33	167.65	44
98.13	25.25	53
14.50	2.52	221
26.79	5.62	201
38.82	2.69	1753

44.08	5.58	166
38.01	14.20	60
13.04	5.68	58
43.63	9.21	76
28.72	14.36	51
29.22	6.11	109
23.26	3.99	152
19.65	2.22	332
20.18	2.69	342
33.07	4.29	186
19.16	8.06	115
33.49	6.79	104
56.27	14.52	60
94.05	19.72	117
83.34	12.75	171
43.44	6.78	945
40.36	6.32	587
79.43	28.39	780
29.57	6.42	76
23.37	6.79	91
29.36	4.63	214
62.29	12.19	81
32.71	8.02	68
8.76	3.31	117
9.78	5.25	43
21.85	2.62	246
47.73	6.37	275

45.70	12.19	262
29.26	3.15	648
47.00	5.59	3664
46.44	16.94	221
30.39	8.35	77
18.08	4.24	145
45.51	18.66	175
32.89	9.05	46
41.57	4.73	210
62.39	8.57	819
34.42	19.44	154
43.07	2.18	9552
35.01	10.60	40
51.84	24.80	65
30.00	4.85	284
36.74	10.02	46
79.83	21.57	60
41.39	4.33	847
20.42	2.51	222
58.20	16.91	61
70.41	6.04	902

Table S7. D_e values from OSL dating of sample T3JURB02.

D_e (Gy)	D_e Uncertainty (Gy)	Net T_n signal in response to 10.6 Gy (cts/0.1 s)
37.66	7.69	246
46.91	6.04	277
85.75	30.60	277

8.21	3.41	69
107.53	37.69	106
47.66	9.42	282
22.94	6.40	79
55.04	9.11	140
107.55	9.58	876
156.10	41.10	379
88.91	96.72	123
46.16	7.99	344
68.04	4.30	912
71.36	13.22	581
64.65	8.31	133
61.29	14.47	116
110.85	12.27	749
27.71	3.18	259
84.36	9.02	3313
65.02	37.42	249
41.07	10.15	95
38.63	4.81	520
26.01	1.69	1014
62.42	5.73	1443
50.55	16.66	283
26.43	12.01	88
48.67	8.16	166
124.07	7.82	1778
88.97	5.98	4186
85.46	12.43	224

1
2
3
4
5
6
7
8
9
10
11
12
13
14
15
16
17
18
19
20
21
22
23
24
25
26
27
28
29
30
31
32
33
34
35
36
37
38
39
40
41
42
43
44
45
46
47
48
49
50
51
52
53
54
55
56
57
58
59
60

25.34	2.12	925
52.79	5.80	353
42.10	2.47	1139
72.83	9.46	351
36.19	17.90	312
40.86	6.34	288
88.24	9.08	428
48.42	4.88	484
21.00	7.37	73
100.45	24.80	304
68.51	3.78	4122
20.88	6.89	125
38.57	22.04	125
76.51	70.72	134
44.26	2.24	3369
28.80	5.17	131
29.94	9.50	74
76.24	25.58	84
60.02	3.32	1714
39.73	3.57	470
53.46	7.50	156
115.27	9.49	8317
30.63	7.81	78
36.49	7.31	114
30.27	3.84	314
97.44	6.19	1590
58.11	11.54	135

75.11	19.88	114
77.11	31.21	1219
55.73	5.69	478
22.78	4.07	421
20.48	3.17	126
48.81	9.00	307
50.48	23.41	100
70.74	10.07	335
26.85	14.03	188
33.87	6.83	125
36.40	9.42	213
23.07	5.30	67
89.93	22.32	10618
26.63	5.11	172
73.32	6.72	318
29.77	6.25	219
45.60	33.38	1174
83.81	11.42	206
36.81	3.71	459
59.23	12.62	139
28.09	3.54	184
59.04	3.97	60304
26.98	4.47	192
71.51	20.99	150
34.44	3.22	12389
42.87	5.20	186

Table S8. D_e values from OSL dating of sample T3GUTT01.

D_e (Gy)	D_e Uncertainty (Gy)	Net T_n signal in response to 13.0 Gy (cts/0.1 s)
110.93	13.61	439
67.53	6.86	264
26.13	7.31	60
199.15	22.16	202
21.68	4.10	112
17.04	4.50	68
159.82	20.19	143
74.31	24.20	39
166.36	47.00	60
53.50	12.97	105
122.87	22.62	82
82.40	24.55	45
171.83	62.33	53
153.23	40.27	82
100.09	27.12	130
110.83	17.68	64
201.41	34.21	171
213.10	33.72	105
116.22	20.56	104
149.24	20.51	178
86.68	25.45	62
120.19	28.74	59
56.48	15.94	44
52.73	7.82	170
107.87	31.02	94
107.23	32.20	136

104.01	19.91	82
101.53	29.84	51
132.80	32.17	54
84.52	27.08	155
142.14	33.72	55
49.70	9.01	107
87.93	16.02	75
133.90	41.60	47
52.64	14.17	53
180.86	30.79	87
167.51	18.61	236
45.88	11.53	50
27.24	9.53	48
15.86	5.40	53
41.49	25.92	65
197.77	45.27	123
29.34	13.73	40
101.51	16.45	409
129.73	14.13	210
77.83	39.25	331
107.02	82.09	123
160.77	133.44	71
90.89	24.75	83
51.23	7.71	622
40.24	7.31	130
87.88	30.29	52
57.53	20.53	88

1
2
3
4
5
6
7
8
9
10
11
12
13
14
15
16
17
18
19
20
21
22
23
24
25
26
27
28
29
30
31
32
33
34
35
36
37
38
39
40
41
42
43
44
45
46
47
48
49
50
51
52
53
54
55
56
57
58
59
60

88.71	12.89	97
125.02	9.31	777
83.46	27.48	53
137.31	67.27	115
18.68	3.26	161
88.77	17.29	98
70.56	12.10	53
37.17	11.06	200
112.46	41.81	95
46.95	8.67	118
51.63	20.52	60
142.43	26.22	95
16.13	3.94	61
136.32	33.85	63
44.30	16.19	67
129.55	24.90	226
135.51	35.39	110
127.09	27.78	65
168.48	33.55	67
136.34	27.19	125
123.93	27.57	148
103.04	18.85	111
93.19	21.50	73
155.28	15.29	408
58.29	9.62	128
147.23	20.28	140
74.18	20.58	74

D_e (Gy)	D_e Uncertainty (Gy)	Net T_n signal in response to 12.6 Gy (cts/0.1 s)
113.47	20.60	156
131.97	20.47	89
26.09	1.96	2076
63.49	33.00	63
154.21	34.94	482
115.30	33.58	53
78.13	25.46	49
114.73	33.22	524
39.49	17.98	137
84.83	18.66	110
85.87	25.27	68
36.56	8.52	137
89.31	28.13	113
116.83	9.46	1143
76.36	15.72	117
91.48	27.63	95
75.89	8.11	492
129.13	47.82	578
73.57	29.02	147
63.97	15.49	137
81.22	7.07	669
75.71	16.70	87
129.47	37.55	101
132.34	54.33	136
89.15	34.48	463

Table S9. D_e values from OSL dating of sample T3GUTT03.

77.80	14.26	152
129.67	13.88	159
119.53	16.53	69
147.27	56.91	45
52.07	7.49	563
74.79	14.77	68
35.18	8.36	181
83.91	20.24	79
37.91	4.69	258
59.77	19.57	178
65.96	11.61	143
29.60	13.89	91
132.79	45.75	162
68.59	17.36	104
45.28	8.90	81
70.59	20.88	60
91.44	20.87	62
23.37	8.77	65
57.17	15.42	92
104.32	17.86	122
127.90	19.30	62
51.34	8.37	182
116.46	5.12	5786
30.95	10.59	141
155.76	34.88	72
147.56	50.63	54
57.45	23.40	65
75.22	5.64	451
32.30	10.59	53
71.25	18.98	191
45.07	5.63	405
133.25	27.31	48

1
2
3
4
5
6
7
8
9
10
11
12
13
14
15
16
17
18
19
20
21
22
23
24
25
26
27
28
29
30
31
32
33
34
35
36
37
38
39
40
41
42
43
44
45
46
47
48
49
50
51
52
53
54
55
56
57
58
59
60

1
2
3
4
5
6
7
8
9
10
11
12
13
14
15
16
17
18
19
20
21
22
23
24
25
26
27
28
29
30
31
32
33
34
35
36
37
38
39
40
41
42
43
44
45
46
47
48
49
50
51
52
53
54
55
56
57
58
59
60

73.93	18.27	48
59.34	36.67	263
57.08	15.52	93
8.07	8.15	59
80.91	12.26	164
118.30	25.28	1428
72.32	17.13	162
77.13	14.53	57
82.01	6.67	971
68.75	17.46	64
133.31	18.41	113
81.89	69.06	169
122.88	24.54	71
39.06	5.36	201
65.28	9.16	179
52.76	30.47	136
136.08	26.83	71
35.78	6.01	170
130.68	62.83	48
73.98	11.65	168
39.08	4.36	425
96.96	16.37	59
44.76	19.76	128
52.81	13.03	75
70.02	11.85	52
153.56	25.88	46
19.14	4.12	125
58.16	14.84	69
32.78	5.51	106
57.06	28.35	54
120.24	49.01	141
50.15	11.79	101

39.60	12.59	42
75.16	26.37	58
86.56	14.00	132
157.28	26.70	88
103.95	16.56	455
31.61	7.35	89
144.39	20.00	207
80.96	22.79	44
110.96	17.76	54
126.43	39.29	48
116.37	28.52	49
155.00	36.82	118
64.67	7.51	520

Table S10. D_e values from OSL dating of sample T3ALDO01.

D_e (Gy)	D_e Uncertainty (Gy)	Net T_n signal in response to 12.9 Gy (cts/0.1 s)
89.54	65.50	44
52.95	14.07	129
149.96	40.70	50
17.88	5.01	49
92.05	38.66	141
45.78	14.30	48
205.99	23.26	370
197.11	88.52	72
80.57	20.19	68
123.72	26.30	70
140.75	33.37	65
168.06	112.77	155
40.36	10.34	48
121.99	18.21	218
63.44	15.76	149
128.38	29.64	81

133.43	107.37	69
26.70	6.26	93
186.71	37.31	713
190.99	47.34	45
79.08	19.36	64
175.55	30.69	109
125.97	15.95	265
150.58	28.99	114
137.19	92.72	73
71.78	19.28	61
87.91	34.97	33
15.71	3.44	108
148.12	85.66	47
104.89	14.20	139
141.52	22.66	172
162.23	23.77	92
151.39	69.09	50
17.18	4.26	101
16.30	7.40	62
94.20	39.82	91
84.68	30.89	52
96.91	29.41	51
80.51	15.30	154
48.90	11.63	60
111.86	22.47	56
51.90	10.37	69
197.26	23.24	445
140.05	22.57	177
65.41	26.39	61
76.76	27.54	42
174.54	32.90	60
105.63	7.60	217

75.05	17.13	100
86.33	20.33	48
109.73	24.99	62
64.74	19.51	46
47.26	16.69	80
127.51	31.90	58
60.76	14.38	56
114.94	29.96	73

Table S11. D_e values from OSL dating of sample T3ALDO02.

D_e (Gy)	D_e Uncertainty (Gy)	Net T_n signal in response to 12.9 Gy (cts/0.1 s)
149.06	35.74	48
106.57	21.55	98
119.93	30.94	47
133.63	32.46	38
172.01	72.25	67
53.13	10.26	67
169.46	26.08	114
107.74	62.15	58
113.63	32.79	70
113.31	18.37	863
16.45	4.39	153
70.61	12.47	105
113.08	13.71	1056
179.49	97.68	76
106.60	13.97	1294
56.22	11.92	54
92.24	22.42	113
179.38	25.19	238
102.27	22.24	59
180.07	68.11	52
78.70	20.92	82

168.14	44.15	130
112.33	37.88	127
110.64	21.58	84
227.76	103.37	111
137.13	39.61	50
191.80	38.19	101
56.90	13.80	50
15.42	2.08	243
39.05	11.65	47
26.33	39.52	44
93.91	20.38	46
87.91	11.27	250
67.88	12.66	216
183.49	35.87	51
139.81	38.93	187
278.75	112.63	72
101.17	34.83	59
65.57	7.19	340
65.92	20.42	45
17.33	5.25	84
101.65	31.65	50
89.28	18.62	86
74.77	15.80	81
40.06	14.24	48
192.50	75.34	60
116.62	18.50	84
183.06	81.81	243
203.92	32.47	84
157.24	22.44	86
22.71	8.98	42
116.59	80.79	57
209.58	26.15	362

92.32	40.58	60
20.37	11.29	54
132.75	25.18	71
131.21	52.66	52
74.86	16.07	70
138.40	155.09	94
153.62	27.84	58
107.79	25.48	46
172.87	31.32	89
27.92	9.52	77
190.61	39.71	48